Since January 2020 Elsevier has created a COVID-19 resource centre with free information in English and Mandarin on the novel coronavirus COVID-19. The COVID-19 resource centre is hosted on Elsevier Connect, the company's public news and information website.

Journal of Saudi Chemical Society (2022) **26**, 101528

King Saud University

Journal of Saudi Chemical Society

www.ksu.edu.sa
www.sciencedirect.com

ORIGINAL ARTICLE

Synthesis and characterization of violurate-based Mn(II) and Cu(II) complexes nano-crystallites as DNA-binders and therapeutics agents against SARS-CoV-2 virus

Sami A. Al-Harbi

Chemistry Department, University College in Al-Jamoum, Umm Al-Qura University, Makkah, Saudi Arabia

Received 7 April 2022; revised 25 July 2022; accepted 28 July 2022
Available online 5 August 2022

KEYWORDS

Violuric acid;
Manganese(II) and copper (II) complexes;
Antiviral activity;
SARS-CoV-2 virus;
DNA-binding;
Molecular docking

Abstract Synthesis and structural characterization of nano crystallites of *bis*-violurate-based manganese(II) and copper(II) chelates is the subject of the present study. Analytical data and mass spectra as well as thermal analysis determined the molecular formulas of the present metal chelates. Spectroscopic and magnetic measurements assigned the structural formula of the present violurate metal complexes. The spectroscopic and magnetic investigations along with structural analysis results indicated the square planar geometry of both the Mn(II) and Cu(II) complexes. The structural analysis of the synthesized metal complexes was achieved by processing the PXRD data using specialized software Expo 2014. Spectrophotometeric and viscosity measurements showed that violuric acid and its Mn(II) and Cu(II) complexes successfully bind to DNA with intrinsic binding constants K_b from 38.2×10^5 to 26.4×10^6 M^{-1}. The antiviral activity study displayed that the inhibitory concentrations (IC_{50}) of SARS-CoV-2 by violuric acid and its Mn(II) and Cu(II) complexes are 84.01, 39.58 and 44.86 μM respectively. Molecular docking calculations were performed on the SARS-CoV-2 virus protein and the computed binding energy values are −0.8, −3.860 −5.187 and −4.790, kcal/mol for the native ligand, violuric acid and its Mn(II) and Cu(II) complexes respectively. Insights into the relationship between structures of the current compounds and their degree of reactivity are discussed.

1. Introduction

Severe acute respiratory syndrome corona virus 2 (SARS-CoV-2) has now been proven to be the causative agent of the COVID-19 pandemic, as announced by the World Health Organization (WHO) on March 11, 2020. In this context, the relevant studies reported that one of the ways to eliminate

E-mail address: sadharbi@uqu.edu.sa

Peer review under responsibility of King Saud University.

Production and hosting by Elsevier

https://doi.org/10.1016/j.jscs.2022.101528

SARS-CoV-2 comes from inhibiting the work of some enzymes necessary for the continuation of the life cycle of the corona virus [1,2]. In this regard, some studies have proven the success of Au-complexes in eliminating Corona virus by inhibiting the activity of some vital enzymes such angiotensin-converting enzyme II (ACE 2) [3]. In addition, the Au complexes showed inhibitory activity of the Papain-like protease (PL^{pro}) enzyme, which along with 3-Chymotrypsin-Like Protease ($3CL^{pro}$), are essential for the survival of SARS-CoV-2 virus [4–7]. In this context, the therapeutic use of these gold complexes with a half-maximal inhibitory concentration (IC_{50}) of 4 μM reduced SARS-CoV-2 infection in human cells by 95% after 48 h. [8]. Despite the success of these gold complexes in inhibiting the activity of corona virus, their high toxicity prevented them from being used as treatments against SARS-CoV-2 [1,2]. However, this promising therapeutic use of gold complexes against SARS-CoV-2 has excited chemists and pharmacologists to prepare metal complexes with low toxicity and effective therapeutic potential. Among these metal complexes that have shown a lethal effect against the Corona virus are Re(I) tricarbonyl complexes that acted as 3-Chymotrypsin-like protease ($3CL^{pro}$) inhibitors [1,2]. In the same respect, a series of Bi(III) complexes showed an inhibitory effect on the activity of RNA – responsible for viral replication and thus they were considered replication inhibitors, making them potential therapeutics for SARS-CoV-2 [9]. It should be noted here that the WHO has approved the use of safe antiviral agents that act as inhibitors of SARS-CoV-2 replication in the treatment protocol for COVID-19 [1,2].

A survey in the literature indicates the limited or paucity of experimental studies of the therapeutic uses of metal complexes towards the SARS-CoV-2 [1,2,10–13]. On the other hand, the application of computational docking method to discover the therapeutic ability of metal complexes against SARS-CoV-2 virus indicated the therapeutic potential of many metal complexes [14–18]. In this regard and based on molecular docking calculations a series of the transition metal complexes including metal ions belonging to the three series of transition elements, showed significant antiviral activity against a series of pathogenic viruses, including COVID-19 by inhibiting the entry of the virus into the host cells, the RNA replication process or virus budding processes [16]. In the same respect, the results of the molecular docking calculations of these metal complexes showed their virucidal effect against SARS-CoV-2 by inhibiting the RNA replication of the virus making them therapeutic agents against COVID-19 [18].

It is scientifically proven in the medical and pharmaceutical communities, that the ability to bind any drug with DNA is the initial spark in the therapeutic protocol for many diseases. In this regard, several studies have indicated the ability of several metal complexes to bind to DNA, thus giving them the potential to be used as therapeutic agents. In the same context, a number of scientific reports stated that the therapeutic effect of metal complexes against viruses is due to their binding to the virus protein and the inhibition of its replication and activity [19–24]. The lack of a specific drug to treat infection with the Corona virus requires intensifying the efforts of chemists and pharmacists to discover an effective and safe treatment against SARS-CoV-2, which is responsible for the outbreak of the Corona virus pandemic. In this regard, extensive in vitro investigations to determine the potential of a number of metal complexes as therapeutic agents against SARS-CoV-2 replication will lead to the discovery of an effective and safe treatment for COVID-19.

The occurrence of an oximato functional group in the organic ligand provides multiple possibility of bonding to a metal ion, resulting in the formation of many stereochemical forms of the formed metal-containing compound [25]. One of these oxime-containing organic ligands is violuric acid in which its deprotonated form, violurato anion, forms versatile metallic complexes. In this respect, bis-violurate – based metal complexes exhibited promising biological potentials such as antitumour, antifungal and antibacterial activity [25].

It is worth noting here that iron, copper and manganese are the most abundant trace elements in human cells. Therefore, the use of complexes of these elements as therapeutic agents will provide higher safety aspect over the complexes of other elements. A literature survey indicates the scarcity of use of both Cu(II) and Mn(II) complexes as therapeutic agents against SARS-CoV-2. Accordingly, studying the synthesis and characterization of violurate-based Cu(II) and Mn(II) complexes and examining their therapeutic potential against SARS-CoV-2 will enrich efforts to reach an effective and safe treatment that limits the spread of the Corona epidemic.

The aim of the current study is to synthesize bis-violurate – based manganese(II) and copper(II) complexes and to test them as DNA binders and in vitro as therapeutic agents against SARS-CoV-2 virus.

2. Experimental

2.1. Chemicals and materials

The chemicals used in the current study were obtained from Aldrich and Merck, which are distinguished for the high purity and quality of their products.

2.2. Synthesis of violurate-based Mn(II) and Cu(II) complexes

Both the violurate-based Mn(II) and Cu(II) complexes synthesized according to the following procedure: An ethanolic solution of (20 mL) containing the hydrated $MnCl_2$ or $CuCl_2$ (0.01 M) was added dropwise to the stirred hot ethanolic solution (30 mL) of violuric acid (0.02 M). This reaction mixture was refluxed for 1 h during which a solid colored precipitate was formed. The vessels containing these solid colored products were left to cool to room temperature and then filtered and washed several times with hot ethanol and finally with ether. Drying these metal complexes was performed by keeping them in a desiccator over CaO for one week. The purity of these isolated solid colored metal complexes was confirmed by the analytical data presented in Table 1.

2.3. Synthesis of $[CuL_2BF_2]$ complex

One gram of the synthesized violurate – copper(II) complex was suspended in 50 mL diethyl ether and stirred for half an hour at room temperature. To this stirred mixture 5 mL of boron trifluoride etherate (BF_3OEt_2) dissolved in 50 mL diethyl ether was added dropwise. After 24 h of stirring at room temperature, the black suspension formed was separated

Table 1 Analytical data, mass spectral results, molar conductance, color of violurate – based Mn(II) and Cu(II) complexes.

Complex	Color	*m/z*	Λ_M* Ω^{-1} cm^2 mol^{-1}	Found (Calcd.)			
				%C	%H	%N	%M
1) [MnL_2]	Light pink	366.1	15.33	26.16 (26.15)	1.66 (1.09)	22.55 (22.90)	14.84 (14.96)
2) [CuL_2]	Faint olive green	374.7	16.78	42.34 (25.55)	2.64 (1.06)	18.87 (22.38)	16.77 (16.91)

by filtration which was washed with aqueous methanol solution several times and finally left to dry in a desiccator over CaO for 1 week. Analytical data determined the molecular formula and confirmed the purity of the separated precipitate.

2.4. Physicochemical measurements

DNA-binding studies, investigations of antiviral activity and method of molecular docking calculations are described in the supplementary materials (S1).

3. Results and discussion

3.1. General

Violuric acid is a heterocyclic compound containing pyrimidine nucleus and known also as 6-Hydroxy-5-nitroso-1H-pyr imidine-2,4-dione (H_3L). It is a tribasic acid showing three values of pK_a which are 4.56, 9.60 and 13.10 [26]. The structural features of the parent violuric acid I (Scheme 1) permit the presence of 10 tautomeric forms at room temperature [27]. Based on PM3 calculation the energy difference between the most stable and the second most stable tautomers is 1.59 kcal mol^{-1} [27]. Among these tautomers are **II** and **III** shown in Scheme 1 which can be used as promising chelators.

Despite there are three ionizable protons of a molecule of violuric acid (H_3L), in the present case it behaves like a monobasic acid. Previous studies have reported that the common mode of coordination of the violurate anion to metal ion is the bidentate pattern via the oximato nitrogen and neighboring carbonyl oxygen of the tautomeric form **I** [25]. However, in an ethanolic solution, the interaction of violuric acid and $MnCl_2$ or $CuCl_2$ salts in a stoichiometric ratio 1:2 (metal: Ligand) gave the binary metal complex ML_2; M = Mn(II) or Cu(II). The molecular formulas of the pure isolated complexes were set mainly based on the analytical data (Table 1). In the solid stat, manganese(II) violurate complex appears as beautiful bright pink microcrystalline and copper(II) complex is powder crystals olive green in color. The metal complexes under study show a high degree of stability in the atmospheric ambient conditions. These metal complexes display good solubility only in DMF and DMSO.

Measurements of the molar conductivity in a DMF solution of 0.001 M concentration of the present metal violurate chelates are in the range 17.87–20.56 Ω^{-1} cm^2 mol^{-1} indicating their non-electrolytic nature [28]. This finding points out to the removal of the counter anions (chloride ions) in the form of HCl as a result of their union with the ionizable acidic proton of violuric acid molecule upon complex formation. Accordingly violuric acid behaves as a mono acidic bidentate ligand as previously reported in similar studies [25].

3.2. Mass spectra measurements

To increase the certainty of the molecular formulas that were determined from the analytical data, the mass spectra of the metal violurate complexes in question were measured by electron ionization mass spectrometry (EI-MS) technique. In this regard, the results obtained for the present monovalent violurato metal chelates indicate that the corresponding peaks of the molecular ions (M^+) at *m/z* values (Table 1) highly correspond to the specific molecular formulas based on the analytical information. The *m/z* values in Table 1 indicate the purity and the monomeric nature of the prepared metal violurate chelates. The mass spectrum of manganese(II) violurate complex is shown in Fig. 1, while the corresponding EI-MS chart of copper(II) violurate complex is presented in the Supplementary Information S2.

3.3. Thermal analysis

3.3.1. TGA and DTG measurements

Thermal analysis is a practical technique that supports the results of elemental analysis to determine the molecular formula of metallic complexes. From this point of view, the thermal analysis of the violurate – based metal chelates under

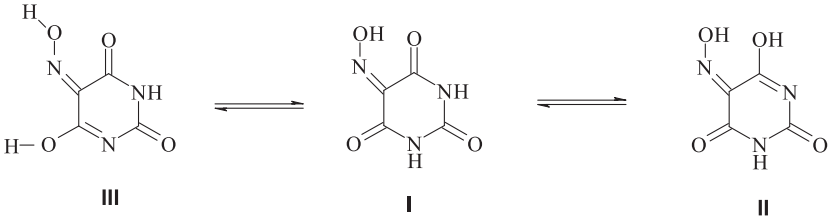

Scheme 1 Possible tautomeric equilibrium of the parent violuric acid I.

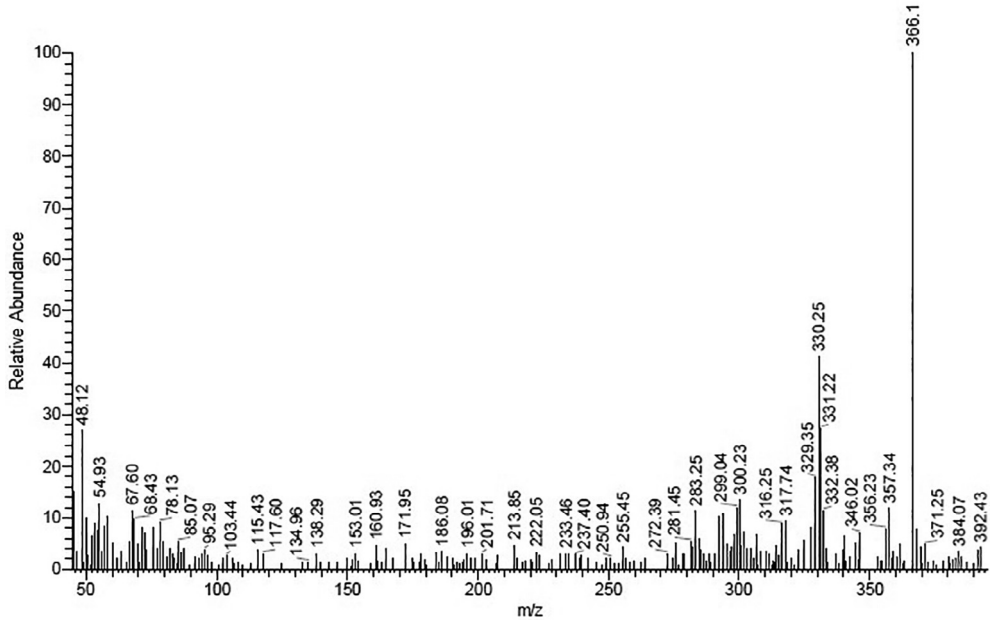

Fig. 1 Mass spectrum of violurate – based Mn(II) complex.

study was studied. In this regard TGA and DTG measurements were performed within the temperature range 50–1000 °C in an N_2 atmosphere. The resulting thermograms are included in the Supplementary Information S3 and S4 while the relevant pyrolysis information is recorded in the Table 2.

Investigation the thermograms of the present metal violurate complexes shows that the pyrolysis proceeds in three successive phases. The first stage that represents the initial weight loss starts at relatively high temperature i.e. 180–245 °C with DGT_{max} peaks at 210 and 205 °C. This thermal behavior indicates the absence of any type of water content and confirms the anhydrous nature of these metal complexes in accordance with the analytical data. Comparison the theoretical (39.34–42.08%) and practical (39.00–41.50%) weight loss values for this stage indicates the thermal degradation corresponding to the partial loss in the organic content of the metal complex.

Pyrolysis of the organic content continues in the second phase of thermal decomposition, which is accompanied by weight loss that falls in the temperature range 210–450 °C. The corresponding DGT_{max} peaks appear at 385 and 380 °C for manganese(II) and copper(II) complexes respectively.

The final pyrolysis stage saw the complete thermal removal of the remaining organic moiety with the concomitant formation of metal oxide (MnO_2 and CuO) as a residual from the overall thermal degradation process of the investigated metal complexes. Theoretical and experimental values for the formed metal oxides are in good agreement based on the percentage of metal content determined by the elemental analysis technique as shown in Table 1.

3.3.2. Kinetic and thermodynamic coefficients determination

Further elucidation the thermal nature of the present violurate-based Mn(II) and Cu(II) complexes can be obtained from the determination of the kinetic and thermodynamic parameters of the three successive pyrolysis steps. To achieve this goal, the Costa-Redefine (CR) [29] and Horowitz-Metzger (HM) [30] approaches were used for calculating the activation energy (E_a), pre-exponential factor (A), and thermodynamic parameters namely ΔH^*, ΔG^* and ΔS^* and the obtained data are collected in Table 3. In the same respect, the relevant data derived from the analysis of TGA and DTG curves for both Mn(II) and Cu(II) complexes based on the CR and HM approaches are represented in Figs. 2 and 3 in the case of first step, while the corresponding plots for the second and third steps are included in S5– S8. Some relations including Boltzmann's (k) and Plank's (h) constants have also been used to calculate the thermodynamic factors such as ΔH^*, ΔG^* and ΔS^* as shown in the following equations:

Table 2 Thermal analysis data of–based violurate Mn(II) and Cu(II) complexes.

*Complex	Temperature °C	DTG_{max} °C	% Weight loss Found (Calcd.)	Species formed
1) $[MnL_2]$	190–245	210	39.00(39.34)	[(MnL]
	245–450	385	12.50(13.77)	$[(MnL_{(0.65)}]$
	450–570	530	25.50(25.57)	MnO_2
2) $[CuL_2]$	180–210	205	41.50(42.08)	$[CuL_{(0.95)}]$
	210–420	380	20.50(20.04)	$[CuL_{(0.45)}]$
	420–550	495	17.50(17.33)	CuO

Table 3 Thermal parameters for the three pyrolysis stages of violurate-based Cu(II) and Mn(II) complexes.

Comp.	Step	Method	E_a (KJ mol^{-1})	A (s^{-1})	ΔS^* (J mol^{-1}.K^{-1})	ΔH^* (KJ mol^{-1})	ΔG^* (KJ mol^{-1})	R^2
[CuL_2]	1st	CR	15.54529	0.108421	−268.557	10.92683	160.1117	0.99464
		HM	25.15972	1.383416	−247.382	20.54439	157.8727	0.99935
	2nd	CR	38.80254	0.82076	−253.774	32.8956	213.1971	0.9502
		HM	50.73895	8.08310	−234.757	44.83201	211.6226	0.9738
	3rd	CR	121.2100	8.36×10^5	−0.1391	115.0400	218.3400	0.9863
		HM	165.5000	9.08×10^8	−0.0819	158.6200	226.3400	0.9875
[MnL_2]	1st	CR	16.96678	0.130014	−267.296	12.20835	165.1921	0.9950
		HM	27.0073	1.673818	−246.071	22.23765	163.4061	0.9974
	2nd	CR	17.0500	3.62×10^{-3}	−0.2990	11.0300	225.3216	0.9526
		HM	29.1700	5.24×10^{-2}	−0.2768	23.1500	223.6500	0.9857
	3rd	CR	111.420	1.16×10^5	−0.1563	104.65	232.1100	0.9758
		HM	128.570	1.64×10^6	−0.1344	121.72	232.3100	0.9765

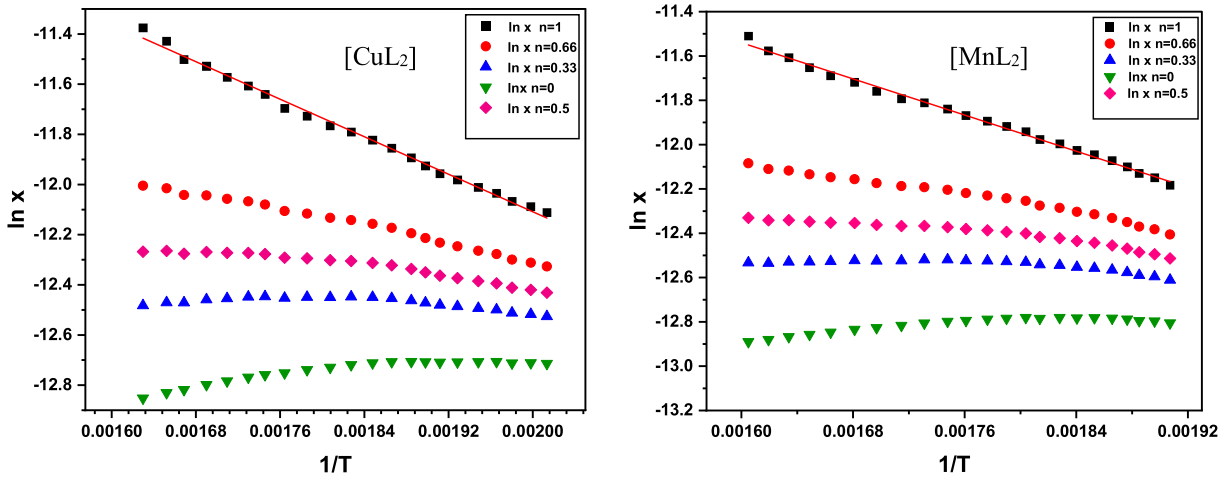

Fig. 2 Coats–Redfern plots of 1st pyrolysis step of violurate-based Cu(II) and Mn(II) complexes.

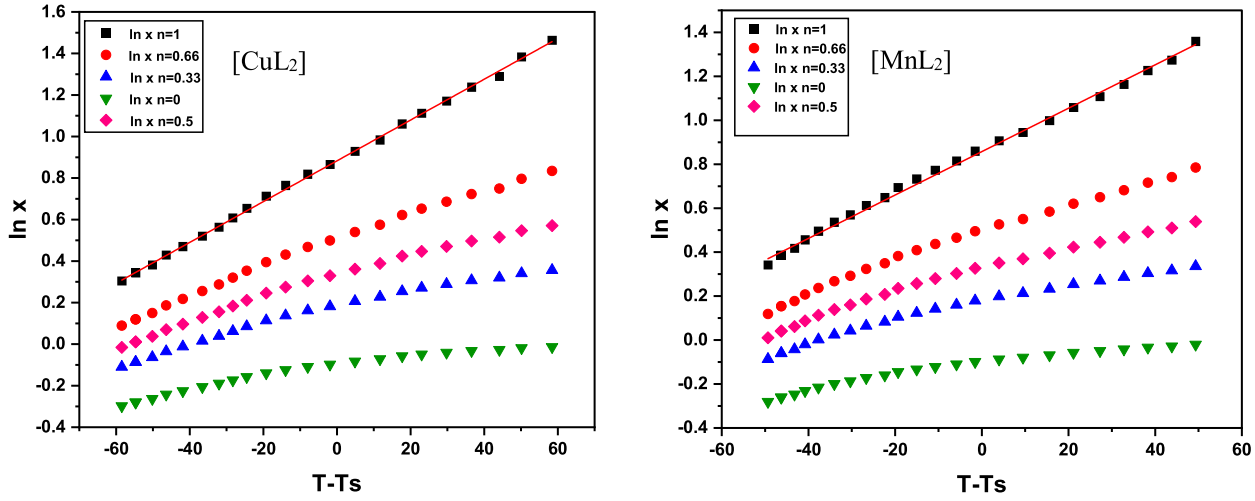

Fig. 3 Horowitz-Metzger (HM) plots of the 1st step pyrolysis step of violurate-based Cu(II) and Mn(II) complexes.

$$\Delta H^{*} = E_a - RT$$

$$\Delta S^{*} = R[ln(Ah/kT) - 1].$$

$$G^{*} = \Delta H^{*} - T\Delta S^{*}.$$

By examining the data given in Table 3, the following facts can be drawn out:

i) There is a marked difference in the average values of the total activation energy for the complete pyrolysis of the violurate-based Mn(II) and Cu(II) complexes. This result can be attributed to the difference in the radii lengths of the Cu(II) and Mn(II) ions. Since the radius of the copper(II) ion is shorter than that of the manganese(II) ion, a stronger bonding between the ligand and the copper(II) ion is expected here. Accordingly, the activation energy is expected to be higher for Cu (II) complex than for Mn(II) complex and this is the case for the data presented in Table 3. However, the E_a values indicate the thermal stability of present metal complexes due to the strong bonding between the monobasic violurate anions and Mn(II) and Cu(II) ions.
ii) The negative sign of ΔS^{*} (Table 3) indicates that the current pyrolysis process proceeds slowly and the reactants are less ordered than the activated complexes [31]. In the same context, negative values of ΔS^{*} can be traced back to the low value of A and possibly due to the non-spontaneous behavior of the studied pyrolysis steps [32]. This interpretation is supported by the positive value of Gibbs free energy ΔG^{*} of the studied thermal decomposition step for the violurate-based Mn(II) and Cu(II) chelates [33]. In the same respect, the calculated positive values of ΔH^{*} indicate that the current pyrolysis processes proceed in an endothermic pattern.
iii) The correlation coefficients (R^2) of the Arrhenius plots for this thermal degradation steps for both Mn(II) and Cu(II) complexes are in the range 0.9502–0.9995, indicative of good agreement with the linear function.
iv) The convergence of the thermodynamic and kinetic coefficients values determined by both Costa-Redefine and Horowitz-Metzger methods confirms the accuracy of the results.
v) First-order kinetics (n = 1) is the pattern of kinetics of pyrolysis reactions for all phases of the two metal complexes under study.

3.4. Verification of the coordination pattern

FTIR spectra of violuric acid and its Mn(II) and Cu(II) chelates were recorded to verify the coordination mode and the related charts are given in S9-S12. The frequencies of characteristic groups of the free violuric acid are tabulated in Table 4. The distinctive stretching vibrations appear at 3450 (broad), 1760 (strong) and 1595 cm^{-1} (strong) are assignable to υ (OH), υ(C═O), and υ(C═N) of the oximato linkage respectively [34]. The broad pattern of the υ(OH) band and its frequency value indicate the presence of a hydrogen bond in the free violuric acid molecule [34,35].

Previous studies demonstrated that violuric acid exhibits many tautomeric forms as shown in scheme 1 because the energy difference between the most stable and the second most stable tautomers is 1.59 kcal mol^{-1} [25]. These structural features of violuric acid lead to different modes of coordination to the metal ion. In this regard, violurate Mn(II) complex was formed as a result of interaction of Mn(II) ion with the tautomer **I** (Scheme 1) through the donor oxygen atoms of oximato group and carbonyl oxygen neighboring to oxime linkage. This mode of coordination has led to the formation of six–membered chelate ring. The validity of this explanation can be inferred from the fact that the spectrum of Mn(II) violurate displays the stretching frequency of the υ(N—O) band at wavenumber value of 1200 cm^{-1}. The current case is comparable to the reported bands for υ(N—O) that appear at 1171 and 1143 cm^{-1} for coordinating oximato-oxygen in nickel(II) and copper(II) complexes [36,37]. As shown in the spectrum of the free violuric acid the υ(N—O) band is located at wavenumber value (1240 cm^{-1}) higher than in the case of Mn(II) complex. It is worth noting here that the bonding of the oxime group to the metal ion through oxygen would reduce the double bond character of the (N—O) bond and thus reduce its stretching vibration frequency [38]. However, the *O,O*-bidentate coordination mode of violurate anion with formation of a six-membered chelate ring has been reported in the case of a *bis*-violurate Sr(II) complex [39].

As regards violurate–based copper(II) complex, its FTIR spectrum displays different vibrations from what is found in the manganese(II) violurate complex, which indicates the different pattern of the coordination in this metal complex. Of these vibrational differences is the observed higher wavenumber for υ(N—O), 1270 cm^{-1}, in the case of Cu(II) complex as compared to that of free violuric acid and Mn(II) violurate complex. This is a vibrational evidence for oximato nitrogen coordination to Cu(II) ion in the five membered chelate ring [40]. Another spectral difference in the spectrum of the copper complex is the appearance of the broad, medium intensity band at 3350 similar to that observed in the free violuric acid but shifted to lower wavenumber and assignable to OH of υ (O—H...O) of the hydrogen bond [35,41]. This finding supports the formation of the copper(II) violurate complex through the reaction of the Cu(II) ion with tautomeric form **II** or **III** (Scheme 1).

Table 4 FTIR spectral data (cm^{-1}) of violuric acid and its Mn(II) and Cu(II) chelates.

Compound	υ(OH)	υ(C═O)	υ(C═N)	υ(N—O)	υ(*N*-M)	υ(O-M)
VA	3450	1760	1595	1240		
MnL_2	–	1710	1595	1200	550	480
CuL_2	3420	1720	1610	1290	550	470
CuL_2BF_2	–	1720	1610	1290	550	470

VA is Violuric acid and L is violurate anion.

To confirm the non involvement of the oximato OH group (=*N*-OH) in complex formation and the presence of a hydrogen bond in the existing violurate–based Cu(II) compound, one gram of this complex is suspended in ether and then treated by BF_3OEt_2 [42]. Interaction of $[CuL_2]$ with BF_3OEt_2 resulted in the formation of $[CuL_2BF_2]$ that is more stable because it contains a bridge of O–BF_2–O. The spectrum of $[CuL_2BF_2]$ exhibits similar vibrations to $[CuL_2]$ in addition to a new weak band at 1180 and other strong peak at 809 cm^{-1} which are ascribed to B–O stretching modes [37]. Other weak bands observed at 1040 and 1005 cm^{-1} are attributed to the B–F stretches of the BF_2 derivative [43].

In the same regard, the OH-deformation mode of (=*N*-OH) is known to appear around 1300 cm^{-1}, so the medium peak observed at 1280 cm^{-1} in the spectrum of violuric acid is assignable to the OH-deformation stretching mode [34]. In the spectrum of $[CuL_2]$, this peak appears at almost the same position as in the case of free violuric acid indicating that the oximato OH group (=*N*-OH) is not involved in the complex formation. On the other hand, the OH deformation peak disappeared in the spectrum of $[MnL_2]$, indicating the participation of OH in the complex formation. This interpretation is consistent with the present results of structural analysis by X-ray diffraction as described below.

The formation of the hydrogen bond in the case of the copper(II) complex led to the formation of macrocyclic in which two of its members are hydrogen bonds. The ability of the macrocyclic chelated ring system to assimilate the Cu(II) ion into its central cavity may be easier than in the case of the Mn(II) ion because the Cu(II) ion has a smaller size than the Mn(II) ion.

The spectra of Cu(II) and Mn(II) violurate display new peaks at 550 and 470–480 cm^{-1} attributable to υ(M–N) and υ(M–O) which are additional spectral evidence for the formation of these metal chelates [34].

Based on the results obtained during this work so far, it is possible to visualize the structural formulas of the metal complexes under study in Scheme 2.

3.5. Stereochemistry diagnostics

Measurements of both electromagnetic spectra (in the ultraviolet and visible regions) and magnetic properties of transition metal complexes are commonly used techniques to determine the stereochemistry and the electronic properties of the metal complex. In this context, the room temperature spectral measurements were performed for DMF solution of violuric acid the Mn(II) and Cu(II) violurate and the recorded spectral data are given as charts in S13 - S15. The electronic absorption spectrum of violuric acid exhibits two distinctive bands at 340 and 410 nm. The spectra of violurate – Mn(II) and Cu (II) complexes show these transitions at 370 and 415 nm. The spectral activity of the uncomplexed monovalent violurate anion is due to the $n \rightarrow \pi^*$ electronic transition [44].

Regarding the manganese(II) violurate complex, Mn(II) is known to exist in its mononuclear complexes, mostly in the high spin state where S = 5/2 of the ^6S ground term. A survey of the literature indicates that the presence of Mn(II) in its complexes in the low - spin state is rare, and the reported cases are found to be in the square-planar coordination geometry [45–49]. The recorded spectrum of the synthesized Mn(II) violurate complex exhibits two absorption peaks at 580 and 690 nm arising from $^4A_{1g} \rightarrow {}^4E_g$ and $^4A_{1g} \rightarrow {}^4B_{1g}$ transitions characteristic to square-planar geometry of the four-coordinated Mn(II) ion [46–49].

Concerning the Cu(II) violurate its UV–vis spectrum shows three d-d spin allowed transitions at wavenumber values of 560, 595 and 685 nm assignable to $^2B_{1g} \rightarrow {}^2B_{2g}$, $^2B_{1g} \rightarrow {}^2A_{1g}$ and $^2B_{1g} \rightarrow {}^2E_g$, respectively [50–52]. These spectral features are characteristic to the square-planar geometry of the four-coordinated Cu(II) complexes [53,54]. Confirmation of this result is based on the fact that no electronic transitions were observed at a wavenumber value below 100,000 cm^{-1} which confirms the exclusion of the tetrahedral or the pseudo-tetrahedral geometry of the present Cu(II) violurate complex [50].

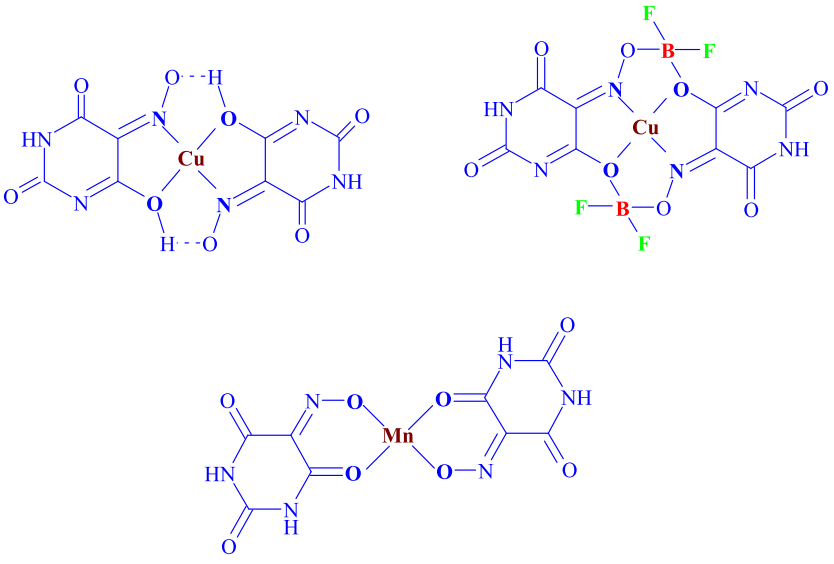

Scheme 2 Molecular Structural visualization of violurate – based Mn(II) and Cu(II) complexes.

The effective magnetic moment value of the present Mn(II) violurate chelate is 4.16 BM characteristic to three unpaired electrons in a dsp^2 hybridization conformation and confirms the square – planar stereochemistry of this Mn(II) complex. In the same regard, the experimental magnetic moment of the violurate – based Cu(II) complex is 1.97 BM indicating the magnetically dilute environment around copper(II) ion.

EPR spectra are complementing spectroscopic technique for determining the stereochemistry of metal complexes. Accordingly the X-band EPR spectra of the current violurate – based Mn(II) and Cu(II) complexes were recorded for the polycrystalline samples at ambient temperature (22 °C) and the relevant charts are included in S16. The spectral features of the studied mineral complexes are characterized by the type of axial symmetry and show two values of g at magnetic field strengths 2400 and 3200 Gauss and can be assigned to $g_{||}$ and $g_{\perp}$.

The computed values of $g_{||}$ and $g_{\perp}$ are 2.312 and 2.051 respectively for Mn(II) complex and 2.192 and 2.044 in the case of Cu(II) complex. For the four-coordinated copper(II) complexes the trend $g_{||} > g_{\perp} > 2.0023$ indicates that the d^2_{x-y} orbital is the ground state ($^2B_{1g}$) of the square-planar structure [55,56]. Concerning Mn(II) violurate complex its EPR spectrum indicates that the violurate ligand system maintains the bivalent state of manganese ion in the square planar coordination polyhedron. The calculated g_{av} values are 2.138 and 2.093 for Mn(II) and Cu(II) complexes confirm the covalent character of the metal–ligand bond [57].

3.6. PXRD – structural analysis

In many cases, it is difficult to obtain an appropriate single crystal of the metal complex so that its exact composition can be proven by X-ray structural analysis. Recently, XRD data processing by specialized software has become well established as a scientific technique for the structural determination of microcrystalline sample for metal complexes [58–61].

However, the XRD spectra of the metal violurate chelates were measured and the related PXRD-charts are displayed in Figs. 4 and S17. In this regard the well known software Expo 2014 was used for performing the structural analysis of metal violurate chelates under study.

In the same context the Rietveld refinement approach was used to maximize the fit between the XRD spectroscopic data and the computationally generated data as shown in Figs. 5 and S18.

The obtained results are given in Tables 5–7 where contain crystallographic data and the related structural parameters e.g. selected bond length and bond angles. Both Mn(II) and Cu(II) violurate complexes crystallized in the crystal systems triclinic of the space group *P*1 and monoclinic with space group *P*21/n respectively (Table 5). The corresponding unite cell dimensions in the case of Mn(II) complex are a = 9.538 Å, b = 9.459 Å, c = 7.660 Å, α = 97.967°, β = 90.362° and γ = 100.475°, while for Cu(II) complex the lattice data are a = 15.598 Å, b = 5.503 Å, c = 15.043 Å, α = 90.0°, β = 114.704° and γ = 90.0°. In the same context the bond length and bond angles around Mn(II) and Cu(II) centers in addition to the computed geometrical index τ_4 are tabulated in Tables 6 and 7.

The optimized structure of Mn(II) violurate complex is shown in Fig. 6 in which the donors sites O(1), O(2), O(3) and O(4) are located in corners of the equatorial coordination polyhedron around Mn(II) center. Since the coordination number of this metallic complex is four, the geometry is likely to be either a square planar or a tetrahedron.

However, the present structural analysis date can solve this problem by determining the geometrical index τ_4. By knowing the values of angles around the central metal ion Mn(II) τ_4 can be determined from the relation $\tau_4 = [360 - (\alpha + \beta)]/141$; where α and β are the two largest angles around Mn(II) center [62]. It is known that if the value of τ_4 is zero, then the geometry is ideal square planar while for τ_4 equals 1 the geometry is perfect tetrahedron [62]. In this respect, the computed value of τ_4 is 0.001 approaching zero indicating mostly ideal square-planar stereochemistry.

The crystallites size of the present violurate – based metal complexes were determined by using Scherer-equation:

$$D = \frac{k\lambda}{\beta \cos\theta}$$

where D is the grain size of the particle (nm), k is Scherer constant (k = 0.94), X-ray wavelength (1.54178 Å) was given by λ, β is full width at half maximum (FWHM) of the diffraction peak and θ is the angle of diffraction. The obtained results, which are listed in Tables 6 and 7, indicate that the crystallites size of the manganese(II) and copper(II) complexes are 25.754 and 21.267 nm, respectively.

Concerning the four-coordinated violurate-based Cu(II) complex the four corners of the equatorial plan of the coordination polyhedron around Cu(II) center are occupied by the donor atoms O(1), n(1), O(2) and N(2). As in the case of Mn(II) violurate complex, the given data in Table 7 was uti-

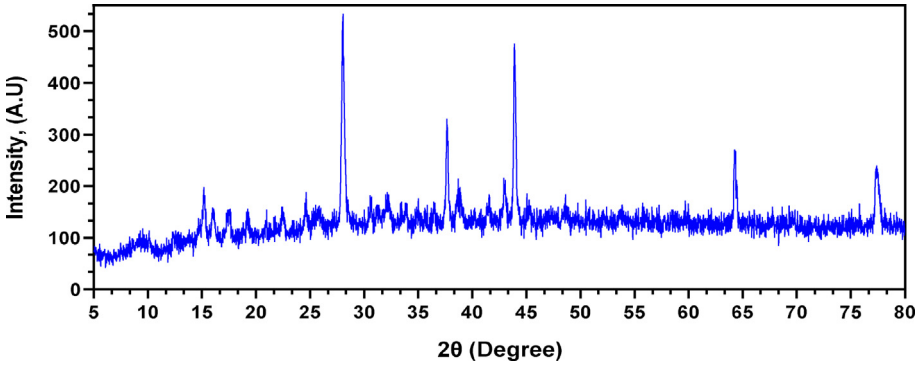

Fig. 4 XRD pattern of violurate –based Mn(II) complex.

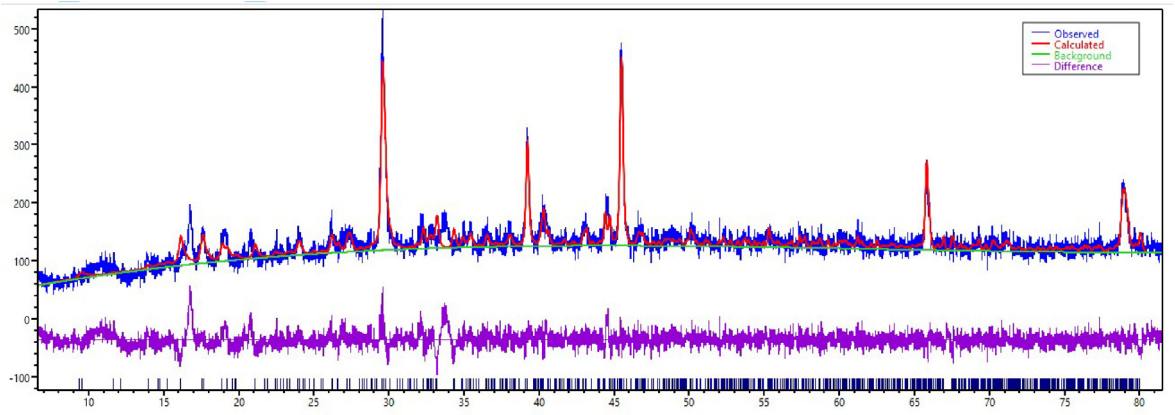

Fig. 5 The maximize fit between the XRD spectroscopic data and the computationally generated data.

Table 5 Crystallographic results of violurate-based Mn(II) and Cu(II) complexes.

Empirical formula	$C_8H_4MnN_6O_8$	$C_8H_2CuN_6O_8$
Formula weight	367.09	373.7
T (K)	279	281
λ (Å)	1.5406	1.5406
Crystal system	Triclinic	Monoclinic
Space group	P−1	P2/m
Centro symmetry	Centric	Acentric
Space Group Number	2	3
Z	2	2
Multiplicity	2	2
Bravais Lattice	P	P
Lattice Symbol	tP	mP
Unit cell dimensions:		
a (Å), *b* (Å), *c* (Å)	9.538, 9.459, 7.660	15.598, 5.503, 15.043
α (°), β (°), γ (°)	97.967, 90.362, 100.475	90.0, 114.704, 90.0
Cell volume ($Å^3$)	672.629	1172.95
Volume per atom ($Å^3$)	14.622	25.499
Calculated density (g/cm^3)	1.812	1.058
θ range for data collection (°)	5 – 80	12 – 80
Total reflection	819	821
Rietveld results:		
Rp	8.303	8.962
Rwp	10.835	11.76
R-Bragg	8.83	23.141
R-F	5.312	3.897

Table 6 Bond angle (Θ) and bond length around Mn(II) center and crystallite size (nm).

Square planar τ_4 = 0.001		Bond Type	Bond distance (Å)
O1-Mn1-O2	93.63	Mn1-O1	1.83531
O1-Mn1-O7	86.36	Mn1-O2	1.84033
O1-Mn1-O8	179.92	Mn1-O7	1.83907
O2-Mn1-O7	179.93	Mn1-O8	1.83386
O2-Mn1-O8	86.45	**Crystallite size**	25.754 nm
O7-Mn1-O8	93.56		

lized to determine the value of the geometrical coefficient. The computed value τ_4 is 0.0006 getting closer to zero pointing to the perfect square-planar geometry and the corresponding optimized structure is given in Fig. 7.

3.7. DNA binding study

It has become known that DNA is the primary drug target for many drugs that treat some diseases, and therefore, understanding the mechanism of binding between DNA and small compounds such as organic ligands and their metal complexes is necessary for the potential therapeutic use of these substances.

3.7.1. Spectral study

The spectral activity of the DNA is due to its structure, which includes a chromophore consisting of purine and pyrimidine

Table 7 Bond angle (Θ) and bond length (Å) around Cu(II) center and crystallite size (nm).

Square planar τ_4 = 0.0006		Bond Type	Bond distance (Å)
O5-Cu1-N5	87.35	O5-Cu1	1.72657
O5-Cu1-O7	179.96	N5-Cu1	1.84717
O5-Cu1-N6	92.64	N6-Cu1	1.84691
N5-Cu1-O7	92.61	O7-Cu1	1.72571
N5-Cu1-N6	179.95	**Crystallite size**	21.267 nm
O7-Cu1-N6	87.40		

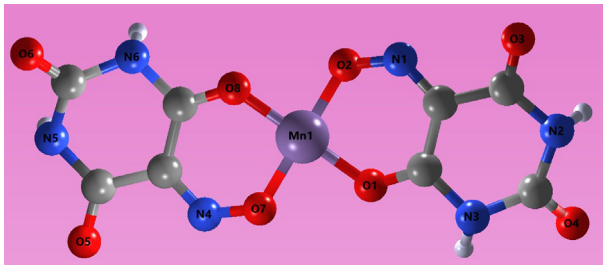

Fig. 6 The optimized structure of violurate – based Mn(II) complex, hydrogen atoms have been omitted for clarity.

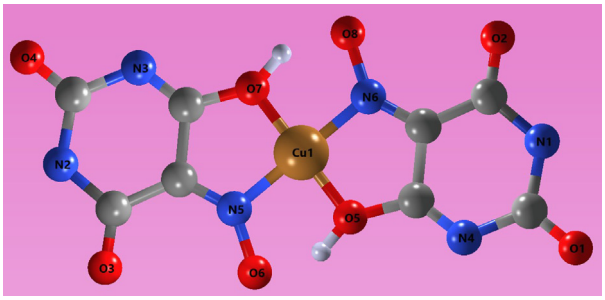

Fig. 7 The optimized structure of violurate – based Cu(II), hydrogen atoms have been omitted for clarity.

rings. These structural properties allow DNA to absorb light well in the ultraviolet and visible regions. Accordingly, the interaction of DNA and its binding to another small molecule can be studied by spectrophotometry. The scientific literature reported that interaction of DNA with a small molecule such as a metal complex or organic ligand may cause hypochromism or hyperchromism accompanied by a bathochromic or hypsochromic shift in the electronic absorption spectra of these substances [63]. The shape of the spectrogram resulting from the increased addition of DNA to a constant concentration of ligand or metallic complex can determine the mode of DNA binding. In this context, if the spectrum shows hypochromism (a decrease in the absorbance) the binding mode of DNA is the intercalation while the presence of hyperchromism (an increase in the absorbance) indicates the groove/electrostatic binding mode [64].

In the present work, spectrophotometeric titrations experiments were performed using a constant concentration (20 μM) of violuric acid and its Mn(II) and Cu(II) complexes treated with increments (5–45 μM) of CT-DNA solution and the resulting spectral changes are shown in Figs. 8, 10 and S19. All the tests conducted at 22 °C in presence of a tris-HCl buffer (pH = 7.6). DNA purity was ascertained by spectrophotometry under ongoing experimental conditions. The obtained spectrum shows the two characteristic absorption bands of protein-free DNA at 260 and 280 nm in a ratio of 1.9:1 [65]. By knowing the absorptivity coefficient value of 6600 M^{-1} cm^{-1} at 260 nm the concentration of DNA per nucleotide was determined [66].

In the absence of ct-DNA the absorption spectra of violuric acid and its metal chelates display-one well-resolved band at 311 nm. The high energy band observed at the wavelength of 311 nm is attributed to the internal ligand charge transfer transitions and is assigned to the $\pi \rightarrow \pi^*$ transition. Addition of CT-DNA to solution of the studied compounds leads to a marked hypochromism of 5.323% without a change in the band position for Cu(II) complex (S19). The same hypochromism of 15.09% with hypsochromic shift (1 nm) is observed for Mn(II) complex (Fig. 9) and indicative of stabilization of the DNA helix. On the other hand, the spectrum of violuric acid showed a significant hyperchromic effect of about 19.89% and no change occurred in the band position as shown in the Fig. 10.

The observed hypochromicity in the spectrograms of Mn (II) and Cu(II) indicates that these metal chelates bind to CT-DNA via the intercalation mode [67,68]. The present spectral features are consistent with that seen for many Metallo-intercalators indicating that these violurate -based metal chelates bind strongly to DNA via the intercalating mode [67,68]. With respect to violuric acid the observed hyperchromism could be due to non-covalent synergistic reactions such as electrostatic, hydrogen and groove bonding along the outer portion of the DNA helix. This interpretation finds support from the observation that the absorption site at 311 nm (Table 8) in the spectrum of violuric acid does not change when a CT-DNA solution is added [69].

Quantitative comparison of the binding strength of violuric acid and its Mn(II) and Cu(II) complexes with DNA can be

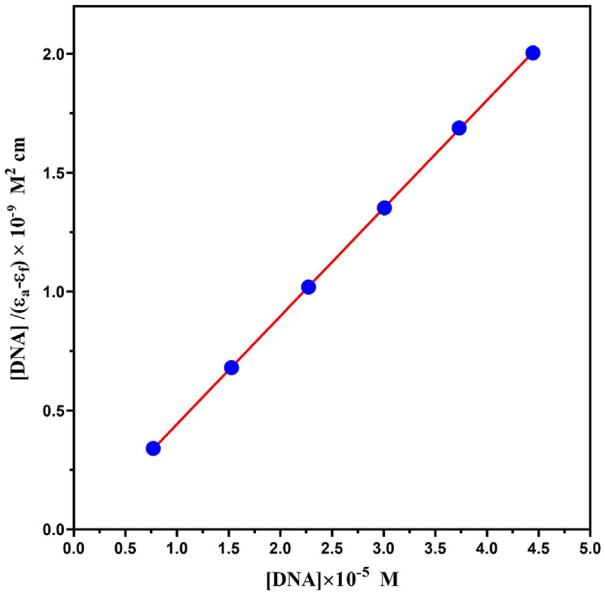

Fig. 8 Plot of $[DNA]/(\varepsilon_a - \varepsilon_f)$ *versus* [DNA] for the DNA binding assay of Mn(II) complex.

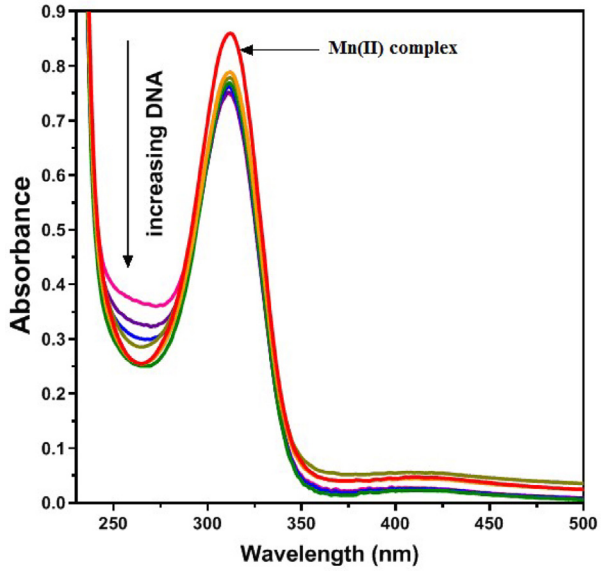

Fig. 9 Spectrograph of the spectrophotometeric titration of manganese(II) complex (20 μM) and ct-DNA (5–45 μM) in Tris-HCl buffer (pH = 7.2).

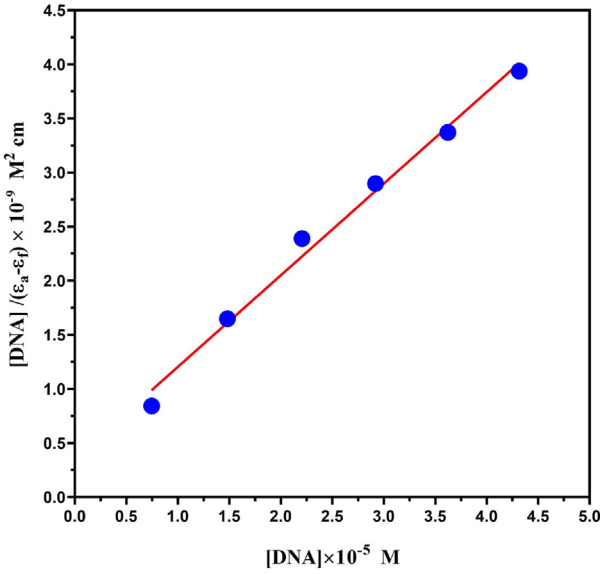

Fig. 10 Plot of [DNA]/($\varepsilon_a - \varepsilon_f$) *versus* [DNA] for the DNA binding assay of violuric acid.

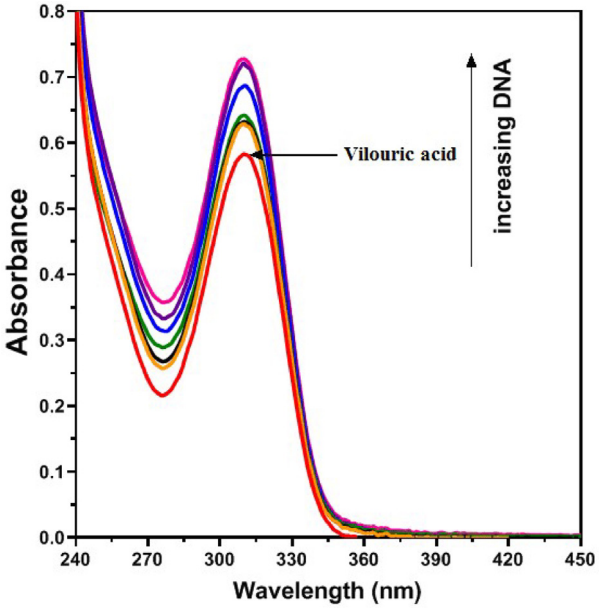

Fig. 11 Spectrograph of the spectrophotometeric titration of violuric acid (20 μM) and ct-DNA (5–45 μM) in Tris-HCl buffer (pH = 7.2).

Table 8 Binding constant data for complexes and ligand.

Compound	K_b	$_{max}\lambda$	$\Delta\lambda^{max}$	%hypo
Mn(II) complex	26.4×10^6	312	1	15.09
Cu(II) complex	$\times 0.27\ 10^6$	311	0	4.49
				hyper%
Violuric acid	38.2×10^5	310	0	19.89

achieved by determining their intrinsic binding constants with CT-DNA.

Quantitative comparison of the degree of binding of the compounds under study with DNA can be achieved by determining their intrinsic binding constants (k_b) with CT-DNA based on the spectrophotometeric titration results and using the Benesi – Hildebrand relation [70]:

$$\frac{[DNA]}{(\varepsilon_a - \varepsilon_f)} = \frac{[DNA]}{(\varepsilon_b - \varepsilon_f)} + \frac{1}{k_b(\varepsilon_b - \varepsilon_f)}$$

The graphical representation between [DNA]/($\varepsilon_a - \varepsilon_f$) on the y–axis and [DNA] on the x–axis gives the plot in Figs. 9, 11 and S20 from which the slope to y-intercept ratio is equal to K_b. and the obtained data are listed in Table 8. ε_f and ε_b are the extinction coefficients of the free and bound complex to DNA respectively.

Table 8 shows that the calculated intrinsic binding constants are 2.38×10^5, 15.09×10^6 and 5.32×10^6 M^{-1} for violuric acid, Mn(II) and Cu(II) chelates respectively. Therefore the binding strength of violuric acid and its metal chelates with ct-DNA follows the sequence Mn(II) > Cu(II) > violuric acid. The question now is why the calculated K_b in the case of violuric acid is lower than in the case of its Mn(II) and Cu(II) chelates? This may be attributed to the different binding pattern in the case of metal complexes (intercalation) than in the case of violuric acid (groove/electrostatic). This reasoning finds support from has been stated in the literature that the calculated binding constant (K_b) in the case of groove binder was found to be lower than in the case of classical intercalator [71].

In the same context, the K_b value of the Mn(II) complex is greater than that of the Cu(II) complex which means that the Mn(II) complex forms a more stable complex with the double helix of DAN than that of the Cu(II) complex where the binding mode is intercalation. The reason why the Cu(II) complex forms a less stable complex with DNA than the Mn(II) complex may be attributed to structural reasons. Both Mn(II) and Cu(II) complexes are four coordinate in a square planar geometrical polyhedron. Since the binding mode of these metal complexes is intercalation one expected that two organic bases (coordinative sites widely diffused in many protein and DNA targets) of the double helix of DNA form two covalent-coordinate bonds with the metal ion and consequently the coordination number becomes six. The Mn(II) ion forms a stable six-coordinate complex in the octahedron structure without difficulties while Cu(II) cannot easily form a stable octahedron complex due to the Jahn-Teller effect.

3.7.2. Viscosity titration measurements

The change in the viscosity of the CT-DNA solution as a result of the increased addition of the violuric acid and its manganese (II) and copper(II) chelates gives an indication of the binding affinity of these compounds as well as the type of bonding between them and the DNA [72,73]. An increase the viscosity of the CT-DNA solution is attributed to the classical intercalation of the molecules of these substances under test, as this requires the separation of the DNA base pairs to accommodate these bonding compounds [74]. While, the decrease in the viscosity of the CT-DNA solution with the addition of increasing amounts of the studied compounds is indicative of the partial and/or non-classical intercalation behavior [75].

To further identify the binding mode of the studied compounds with CT-DNA solution, viscosity titration measure-

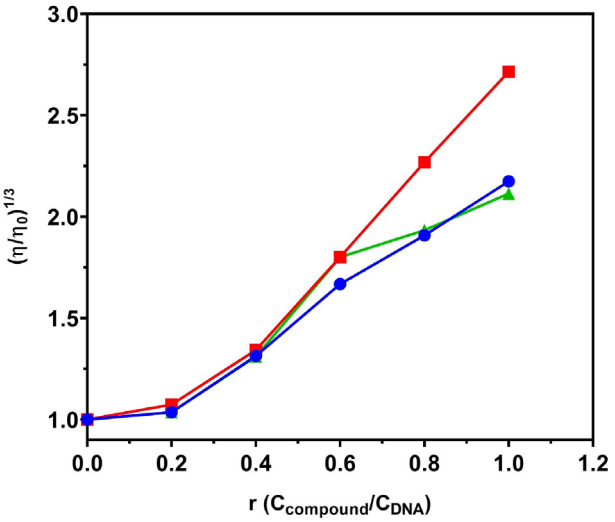

Fig. 12 Effect of the increasing concentrations of violuric acid (▲) and its Mn(II) (■) and Cu(II) (●) chelates on the relative viscosity of CT-DNA solution.

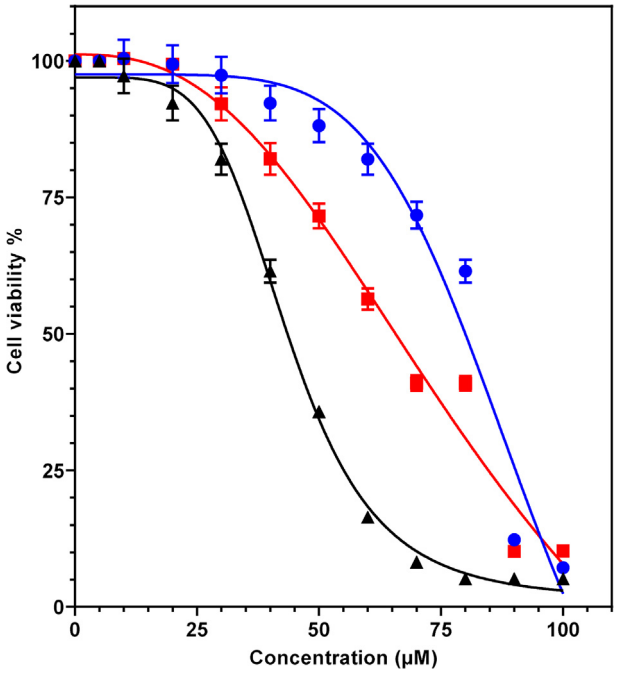

Fig. 13 Cell viability of violuric acid (▲) and its Mn(II) (●) and Cu(II) (■) complexes.

ments were performed at room temperature and the results obtained are shown in the graph of Fig. 12.

Fig. 12 shows that, the viscosity of the CT-DNA solution increases continuously with the increase in the concentrations of the compounds under study. The results presented in the Fig. 12 indicate a convergent increase in the viscosity of the DNA solution in the case of violuric acid and its Cu(II) complex. The larger linear increase in viscosity for the Mn(II) complex indicates a stronger association with CT-DNA in agreement with the results of the current spectroscopic studies. In conclusion the present viscosity titration results are consistent with the intercalation pattern of the interaction of violuric acid and its Mn(II) and Cu(II) chelates with the DNA helix [72].

3.8. Antiviral activity study

Since the outbreak of the Corona virus (Covid-19) pandemic in the world, efforts have joined forces to discover an effective drug against this epidemic, and this has led to the production of some drugs that are currently being evaluated in clinical trials [76,77]. The research strategy has been to focus on traditional small organic molecules or antibody-based therapies [78,79]. Since the metal complexes have proven successful in treating some viral diseases [80], this has encouraged researchers to test some of them in vitro as therapeutic agents against Covid-19 [81–86]. In this context, the metal complexes in the test must be effective and clinically appropriate and showing an acceptable toxicity.

3.8.1. Cytotoxicity

The cytotoxicity of the current candidates as anti SARS-CoV-2 agents, namely violuric acid and its Mn(II) and Cu(II) chelates, was first examined to determine the half-maximal cytotoxic concentration (CC_{50}) in Vero-E6 cells using MTT assay. As shown in the Fig. 13, the obtained results showed that the half-maximal cytotoxic concentration (CC_{50}) values are 43.87, 93.45 and 88.38 μM for the violuric acid its Mn (II) and Cu(II) complexes, respectively. These results indicate that the cytotoxicity of the tested compounds is dose dependent, and therefore the non-toxic doses were used in the subsequent antiviral assays of the compounds under study.

3.8.2. Inhibition of SARS-CoV-2 virus replication

In the going study, a plaque reduction assay used to determine the half-maximal inhibition concentration (IC_{50}) in Vero-E6 cell line model of SARS-CoV-2 virus in presence and absence of violuric acid and its manganese(II) and copper(II) chelates.

Fig. 14 and Table 9 show that the inhibitory concentrations (IC_{50}) of SARS-CoV-2 by violuric acid, Mn(II) and Cu(II) complexes are 84.01, 39.58 and 44.86 μM respectively. These results indicates to dose dependent antiviral behavior and confirm the inhibitory ability of SARS-CoV-2 replication by violuric acid and its manganese(II) and copper(II) chelates. In the same respect the highest inhibition percent of SARS-CoV-2 virus replication of the tested compounds are 20, 49 and 72%, for violuric acid, manganese(II) and copper(II) chelates respectively. It should be noted here that in the blank experiment, in the absence of the compounds under study, no significant decrease in viral inhibition was observed.

It is more appropriate to describe the antiviral activity using the selectivity index ratio CC_{50}/IC_{50}, and the values calculated in Table 9 show approximately the same order as in the case of IC_{50}. However, based on the values of CC_{50}/IC_{50} ratio given in Table 9 the antiviral potency follows the order Mn(II) > Cu(II) > violuric acid. The remarkable discrepancy in the ability of the compounds under study to inhibit SARS-CoV-2 virus replication may be due to the difference in their ability to bind to the virus, as evidenced by DNA binding studies and also demonstrated by molecular docking calculations. As shown in the Table 9, the potential for antiviral activity of Mn(II) and Cu(II) chelates are comparable with other inhi-

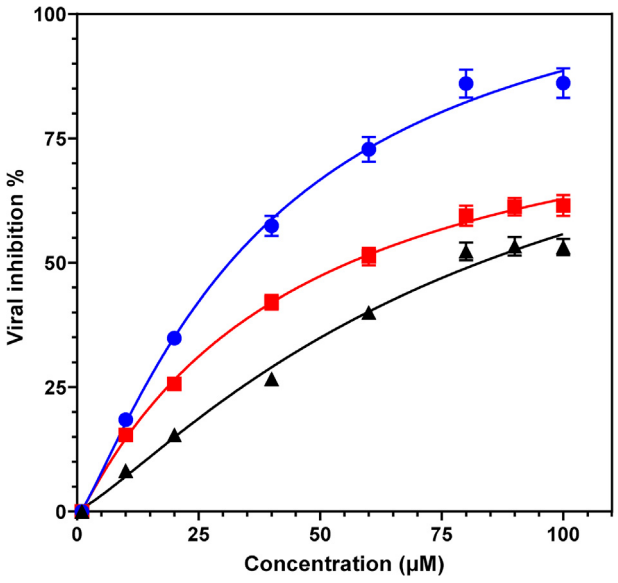

Fig. 14 Viral inhibition activity of violuric acid (▲) and its Mn (II) (●) and Cu(II) (■) complexes.

bitors of SARS-CoV-2 virus replication. In the same regard, Remdesivir remains more effective and safer compared to the compounds listed in Table 9. In the same context, violuric acid exhibits lower antiviral activity than its Mn(II) and Cu(II) complexes and this finding is reported in previous related studies where the metal complexes showed a higher antiviral activity than the single organic ligand [10,14,16]. In general, it is known that the bonding of a metal atom or ion to the organic ligand gives the resulting metal complex molecule biological potentials that do not appear in the case of a single organic ligand [10,14,16].

3.8.3. Molecular docking study

At present, molecular docking calculations are an accepted scientific approach that aids in understanding the way in which metal complexes as therapeutic agents interact with a microbial target substrate. To confirm the experimental antiviral results and to clarify the relationship between the structural features and the potential therapeutic ability of violuric acid and its Mn(II) and Cu(II) complexes, molecular docking calculations were performed on the SARS-CoV-2 virus protein. In this regard, the spike protein (PDB code: 6LZG), of the experimentally studied virus cells (Vero-E6 cells) was selected. The computational chemistry method used is included in the S1 and results of the ongoing molecular docking calculations are given in Table 10, Figs. 15, 16 and S21–S22.

The measure of a drug's success in binding to a biological protein containing an organic ligand is that the drug binds to the protein at the same binding sites as the organic ligand after its exclusion. The current molecular docking calculations demonstrated that the native organic ligand which associated to the spike protein 6LZG binds to this protein via H-acceptor interaction between Asn 322 amino acid residue of chain (A) of spike protein and O(6) of acetamide moiety of this ligand as shown in Fig. 15.

In the same respect 2D and 3D diagrams for the interaction of violuric acid and its Mn(II) and Cu(II) chelates with active sites of 6LZG protein Figs. 16 and S21–S22 showed H-acceptor interaction between Asn 322 amino acid residue of chain (A) of spike protein.

The data in Table 10 point out to the binding - bond distance of the native ligand, violuric acid and its Mn(II) and Cu(II) complexes are 2.82, 2.97, 3.33, and 2.97 Å respectively. In the same regard the computed binding energy values or dock score (Table 10) are −0.8, −3.860, −5.187 and −4.790, kcal/mol for the native ligand, violuric acid and its Mn(II) and Cu(II) complexes respectively.

The overall molecular docking calculations demonstrated that the Mn(II), Cu(II) complexes and violuric acid successfully bind to the spike protein of 6LZG in 3D direction and thus contributed in the inhibition of SARS-CoV-2 virus replication. However, the docking score energy in kcal/mol, RMSD and type of ligand interaction (Table 10) determined the binding affinity of the studied compounds. In the same context, these results indicate that Mn(II) and Cu(II) chelates showed a greater binding affinity than violuric acid in an agreement with the experimental results of the current DNA binding and antiviral study. The current docking analysis showed that Mn(II)-complex has lower docking energy value (−5.1875 kcal/mol) with half-maximal inhibition concentration (IC_{50}) of 39.38 μM and an antiviral activity ratio CC_{50}/IC_{50} of 2.36. These data are comparable with those reported for manganese carbonyl complex as an inhibitor for protein (PDB ID: 5 V13), of SARS-CoV-2 virus which revealed the binding energy of −5.45 kcal/mol and IC_{50} value of 101.07 μM [87]. Concerning Cu(II) violurate complex its antiviral activity data (Table 9) are comparable with Cu(II) - based curcumin complex [88] which showed docking binding energy of −7.06 kcal/mol with IC_{50} value of 6.63 mM for SARS-CoV-2 virus.

Table 9 Cytotoxicity and inhibitors of SARS-CoV-2 virus replication activity of violuric acid and its Mn(II) and Cu(II) complexes and other compounds.

Compound	CC_{50} (μM)	IC_{50} (μM)	CC_{50}/IC_{50}	Reference
Mn(II) complex	93.45	39.58	2.36	This work
Cu(II) complex	88.38	44.86	1.97	This work
Violuric acid	43.87	84.01	0.52	This work
Aubipyc	67	6.3 ± 3.1	10.6	[1]
$TiCp_2Cl_2$	>200	47.3 ± 1.4	>4.2	[1]
Remdesivir	97	0.2 ± 0.05	485	[1]

CC_{50} and IC_{50} are the concentrations of both half-maximal cytotoxic and the half-maximal inhibitory respectively.

Table 10 Docking core and molecular interactions predicted for antiviral binding to 6LZG towards violuric acid and its Mn(II) and Cu(II) chelates.

Compound	Dock Score (kcal/mol)	RMSD	Interaction	Type	Distance	E (kcal/mol)
Mn-complex	−5.187	1.8	ND2 ASN 322 (A) → O16	H-bonding	3.33	−0.8
			O28 → OE1 GLU 312 (A)	H-bonding	2.62	−4.8
			NZ LYS 309 (A) → O4	H-bonding	2.90	−1.0
			OE1 GLU 312 (A) – O2	Ionic	3.89	−0.7
			OE2 GLU 312 (A) – O2	Ionic	3.01	−4.4
			OE1 GLU 312 (A) – O28	Ionic	2.62	−7.6
Cu-complex	−4.790	1.4	ND2 ASN 322 (A) → N11	H-bonding	2.97	−4.5
			O18 → OE1 GLU 312 (A)	H-bonding	2.80	−9.6
			O18 → OE2 GLU 312 (A)	H-bonding	3.48	−0.8
			O23 → O MET 323 (A)	H-bonding	2.76	−6.9
			OE1 GLU 312 (A) – N20	Ionic	3.60	−1.5
Violuric acid	−3.860	1.9	ND2 ASN 322 (A) → O12	H-bonding	2.97	−5.0
NAG (native ligand)			ND2 ASN 322 (A) → O7	H-bonding	2.82	−0.8

3.9. Insights into the relationship between structure and reactivity

Several studies have shown that metal complexes exhibit significant pharmacological effects that are not observed when the parent ligand or the inorganic form of the metal is used alone [89]. In the current work, the compounds under study showed the same trend of biological and pharmacological activity in agreement with the results of similar studies. In this context, the superiority of metal complexes over organic ligands can be understood based on chelation theory [89].

Chelation of the organic ligand to a metal ion blocks the charges on the donor sites and thus reduces the overall charge on the ligand molecule. In addition, the bonding of the ligand to the metal ion also reduces the polarity of the metal ion. These two effects cooperate to increase the susceptibility of cell wall lipids to metal chelates and enhance their penetration across the lipid layer of the cell membrane [90].

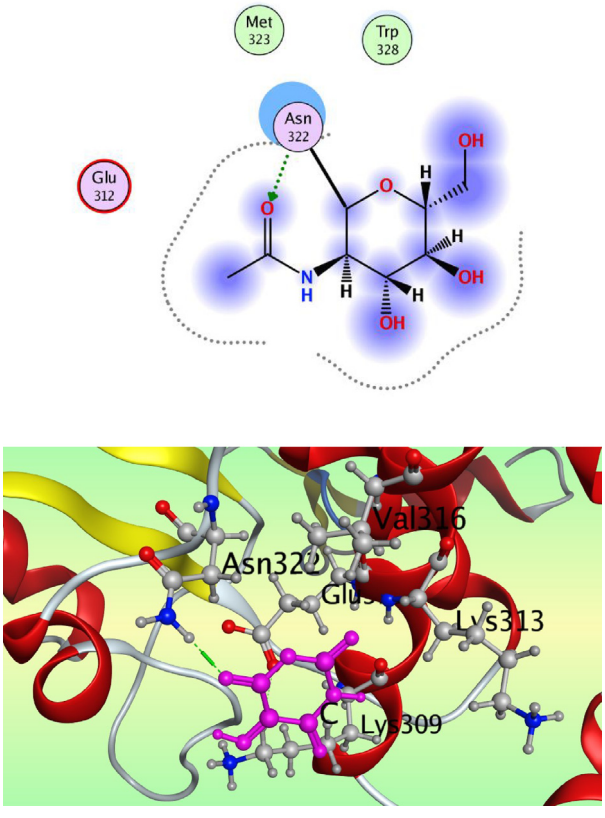

Fig. 15 2D and 3D -molecular interaction of NAG (native ligand) with active sites of 6LZG protein.

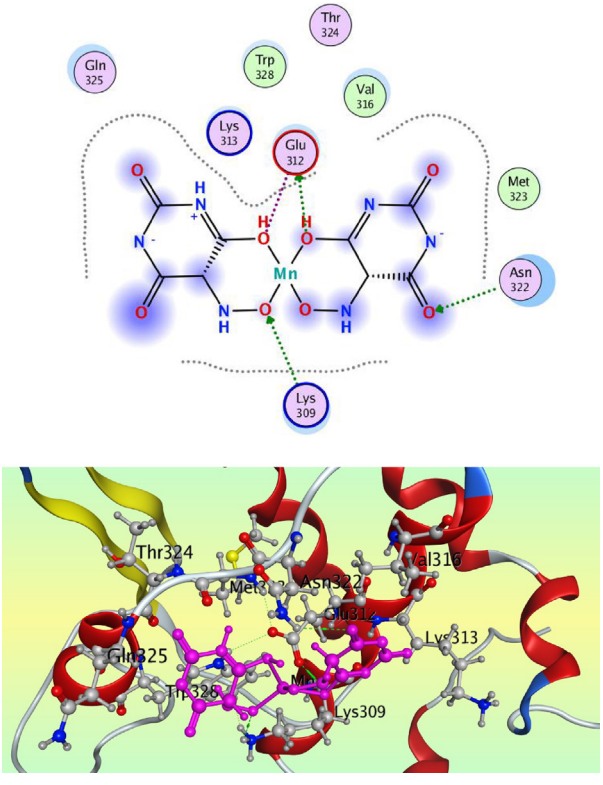

Fig. 16 2D and 3D -molecular interaction of violurate-based Mn(II) complex with active sites of 6LZG protein.

Spectroscopic measurements of the binding of the compounds under study to DNA indicated that violuric acid binds to DNA by non-covalent synergistic reactions while Mn(II) and Cu(II) bind strongly to DNA via the intercalating mode. In intercalation mode covalent bonding between the metal center of metal complex and the bases of DNA helix can not be ruled out. Metallic complexes with a low coordination number as in the case of square planar structure are most suitable for binding with DNA. This is because, the nitrogen donors of the helical bases of DNA can easily bind to the metal center without the need for dissociation energy to provide an empty coordination site on the metal center as in the case of coordinationally saturated metal complexes. Accordingly, the superiority of the Mn(II) complex in the degree of bonding with DND over the Cu(II) complex may be attributed to the degree of stability of the complex resulting from the binding of these complexes to DNA.

Since DNA is rich in nitrogen bases, it is expected that the metal ion of the metal complex will bind to the two helixes and produce hexacoordinated complex in an octahedral structure. Here the degree of stability of the Cu(II) complex with DNA is expected to be lower than in the case of the Mn(II) complex due to the Jahn-Teller effect that reduces the stability of the six coordinate copper(II) complexes.

This discussion can also be applied to explain the antiviral superiority of manganese(II) complex over copper(II) complex against SARS-CoV-2 virus.

4. Conclusion

Violuric acid interacts with Mn(II) and Cu(II) ions in a stoichiometric ratio 1:2 (metal:Ligand) to give the binary metal complex ML_2 where L is violurate monovalent anion and M is Mn(II) or Cu(II) ions. The bis-violurate ligand system coordinates to copper(II) ion via the N_2O_2 coordination chromophore which results in the formation of equatorial macrocycle stabilized by an intramolecular hydrogen bond. The ability of the macrocyclic chelated ring system to accommodate the Cu(II) ion in its central cavity is easier than in the case of Mn(II) due to the smaller size of the Cu(II) ion than the Mn(II) ion. Accordingly, the bis-violurate system binds to Mn (II) ion by the *O,O*-bidentate coordination mode with formation of a six-membered chelate ring. The exact structure of the metal complexes under study was confirmed by processing the XRD- data using the software Expo 2014. Spectroscopic investigations and viscosity measurements indicate the success of the compounds under study in binding to CT-DNA. Intercalation is the binding mode in the case of Mn(II) and Cu(II) complexes while the groove/electrostatic is the binding mode for violuric acid. Based on the results of spectroscopic measurements of the binding of the compounds under study with DNA, it can be concluded that the pattern of binding and type of metal ion control the degree of binding of these compounds to DNA.

The results of cytotoxicity tests for the examined compounds indicate that they are dose-dependent, and non-toxic doses were used in the studied antiviral assays. Molecular docking calculations reported that the native organic ligand present for the studied 6LZG protein from SARS-CoV-2 has lower binding affinity compared to violuric acid and its metal complexes. The overall results (biological assays and computational study) are consistent and emphasize the fact that violuric acid and its Mn(II) and Cu(II) complexes have a virucidal effect in vitro infection of SARS-CoV-2. The results of the study indicate that the Mn(II) complex can be used as a treatment for the COVID-19 pandemic after appropriate in vivo and clinical trials are performed.

Overall, the stability degree of the complex formed between DNA and the metal ion of the present metal complexes demonstrates the superiority of the Mn(II) complex over the Cu(II) complex as a DNA-binder and therapeutic agent against SARS-CoV-2.

Declaration of Competing Interest

The authors declare that they have no known competing financial interests or personal relationships that could have appeared to influence the work reported in this paper.

Acknowledgements

The author would like to thank the Deanship of Scientific Research at Umm Al-Qura University for supporting this work by Grant Code: 19-SCI-1-01-0031.

Appendix A. Supplementary data

Supplementary data to this article can be found online at https://doi.org/10.1016/j.jscs.2022.101528.

References

[1] D. Cirri, A. Pratesi, T. Marzo, L. Messori, Metallo therapeutics for COVID-19. Exploiting metal-based compounds for the discovery of new antiviral drugs, Expert Opin. Drug Discov. 16 (1) (2021) 39–46, https://doi.org/10.1080/17460441.2020.1819236.

[2] J. Karges, S.M. Cohen, Metal Complexes as Antiviral Agents for SARS-CoVID-2, ChemBioChem 22(16) (2021) 2600-2607; https://doi.org/10.1002/cbic.202100186; and references therein.

[3] P. Zhang, L. Zhu, J. Cai, F. Lei, J.-J. Qin, J. Xie, Y.-M. Liu, Y.-C. Zhao, X. Huang, L. Lin, M. Xia, M.-M. Chen, X.u. Cheng, X. Zhang, D. Guo, Y. Peng, Y.-X. Ji, J. Chen, Z.-G. She, Y. Wang, Q. Xu, R. Tan, H. Wang, J. Lin, P. Luo, S. Fu, H. Cai, P. Ye, B. Xiao, W. Mao, L. Liu, Y. Yan, M. Liu, M. Chen, X.-J. Zhang, X. Wang, R.M. Touyz, J. Xia, B.-H. Zhang, X. Huang, Y. Yuan, R. Loomba, P.P. Liu, H. Li, Association of inpatient use of angiotensin-converting enzyme inhibitors and angiotensin II receptor blockers with mortality among patients with hypertension hospitalized with COVID-19, Circ. Res. 126 (12) (2020) 1671–1681.

[4] M. Gil-Moles, U. Basu, R. Büssing, H. Hoffmeister, S. Türck, A. Varchmin, I. Ott, Gold metallodrugs to target coronavirus proteins: inhibitory effects on the spike-ACE2 interaction and on PLpro protease activity by auranofin and gold organometallics, Chem. Eur. J. 26 (66) (2020) 15140–15144.

[5] Y. Chen, Q. Liu, D. Guo, Emerging coronaviruses: genome structure, replication, and pathogenesis, J. Med. Virol. 92 (4) (2020) 418–423, https://doi.org/10.1002/jmv.25681.

[6] D. Shin, R. Mukherjee, D. Grewe, D. Bojkova, K. Baek, A. Bhattacharya, L. Schulz, M. Widera, A.R. Mehdipour, G. Tascher, P.P. Geurink, A. Wilhelm, G.J. van der Heden, H. van Noort, S. Ovaa, K.-P. Müller, K. Knobeloch, B.A. Rajalingam, J.C. Schulman, G. Hummer, S. Ciesek, I. Dikic, Papain-like protease regulates SARS-CoV-2 viral spread and innate

immunity, Nature 587 (7835) (2020) 657–662, https://doi.org/10.1038/s41586-020-2601-5.
[7] M.D. Sacco, C. Ma, P. Lagarias, A. Gao, J.A. Townsend, X. Meng, P. Dube, X. Zhang, Y. Hu, N. Kitamura, B. Hurst, B. Tarbet, M.T. Marty, A. Kolocouris, Y. Xiang, Y. Chen, J. Wang, Structure and inhibition of the SARS-CoV-2 main protease reveal strategy for developing dual inhibitors against Mpro and cathepsin L, Sci. Adv. 6 (50) (2020) eabe0751, https://doi.org/10.1126/sciadv.abe0751.
[8] H.A. Rothan, S. Stone, J. Natekar, P. Kumari, K. Arora, M, Kumar, The FDA-approved gold drug auranofin inhibits novel coronavirus (SARS-COV-2) replication and attenuates inflammation in human cells, Virology 547 (2020) 7–11, https://doi.org/10.1016/j.virol.2020.05.002.
[9] S. Yuan, R. Wang, J.-F.-W. Chan, A.J. Zhang, T. Cheng, K.-K.-H. Chik, Z.-W. Ye, S. Wang, A.-Y. Lee, L. Jin, H. Li, D.-Y. Jin, K.-Y. Yuen, H. Sun, Metallodrug ranitidine bismuth citrate suppresses SARS-CoV-2 replication and relieves virus-associated pneumonia in Syrian hamsters, Nat. Microbiol. 5 (11) (2020) 1439–1448, https://doi.org/10.1038/s41564-020-00802-x.
[10] T. Marzo, L. Messori, A role for metal-based drugs in fighting COVID-19 infection? The case of auranofin, ACS Med. Chem. Lett. 11 (6) (2020) 1067–1068, https://doi.org/10.1021/acsmedchemlett.0c00190.
[11] I. Altaf, M.F. Nadeem, N. Hussain, M. Nawaz, S. Raza, M.A. Shabbir, M.A. Ashraf, M.A. Ali, S. Hassan, M.W. Aziz, N. Matti, M. Ashraf, I. Ulla, S. Fazal, S. Rafique, A. Mehmood, N. Sardar, M.T. Khan, H.M.M. Atique, S. Ashraf, Z. Tahir, N. Mukhtar, T. Yaqub, An in vitro antiviral activity of iodine complexes against SARS-CoV-2, Arch. Microbiol. 203 (7) (2021) 4743–4749, https://doi.org/10.1007/s00203-021-02430-3.
[12] B. Atasever Arslan, B. Kaya, O. Şahin, S. Baday, C.C. Saylan, B. Ülküseven, The iron(III) and nickel(II) complexes with tetradentate thiosemicarbazones. Synthesis, experimental, theoretical characterization, and antiviral effect against SARS-CoV-2, J. Mol. Struct. 1246 (2021) 131166, https://doi.org/10.1016/j.molstruc.2021.131166.
[13] J. Haribabu, S. Srividya, D. Mahendiran, D. Gayathri, V. Venkatramu, N. Bhuvanesh, R. Karvembu, Synthesis of palladium(II) complexes via Michael addition: antiproliferative effects through ROS-mediated mitochondrial apoptosis and docking with SARS-CoV-2, Inorg. Chem. 59 (23) (2020) 17109–17122, https://doi.org/10.1021/acs.inorgchem.0c02373.
[14] K. Ashiq, B. Naureen, S. Ashiq, Metal complexes and their potential therapeutic role against COVID-19: recent developments in drug designing, Sud. J. Med. Sci. 16 (4) (2021) 540–545, https://doi.org/10.18502/sjms.v16i4.9951.
[15] M.C. Vlasiou, K.S. Pafti, Screening possible drug molecules for Covid-19. The example of vanadium(III/IV/V) complex molecules with computational chemistry and molecular docking, Comput. Toxicol. 18 (2021), https://doi.org/10.1016/j.comtox.2021.100157 100157.
[16] M. Pal, D. Musib, M. Roy, Transition metal complexes as potential tools against SARS-CoV-2: an in silico approach, New J. Chem. 45 (4) (2021) 1924–1933, https://doi.org/10.1039/d0nj04578k.
[17] Y.M. Ahmed, M. Omar, G.G. Mohamed, Synthesis, spectroscopic characterization, and thermal studies of novel Schiff base complexes: theoretical simulation studies on coronavirus (COVID-19) using molecular docking, J. Iran. Chem. Soc. 19 (3) (2022) 901–919, https://doi.org/10.1007/s13738-021-02359-w.
[18] K.M. Hashim, E. Manoj, M.P. Kurup, A novel manganese(II) bisthiocarbohydrazone complex: crystal structures, Hirshfeld surface analysis, DFT and molecular docking study with SARS-CoV-2, J. Mol. Struct. 1246 (2021), https://doi.org/10.1016/j.molstruc.2021.131125 131125.
[19] W.A. Wania, E. Jameel, U. Baigc, S. Mumtazuddin, L.T. Huna, Ferroquine and its derivatives: new generation of antimalarial agents, Eur. J. Med. Chem. 101 (2015) 534–551, https://doi.org/10.1016/j.ejmech.2015.07.009.
[20] U. Koch, B. Attenni, S. Malancona, S. Colarusso, I. Conte, M. Di Filippo, S. Harper, B. Pacini, C. Giomini, S. Thomas, I. Incitti, L. Tomei, R. De Francesco, S. Altamura, V.G. Matassa, F. Narjes, 2-(2-Thienyl)-5,6-dihydroxy-4-carboxypyrimidines as inhibitors of the hepatitis C virus NS5B polymerase: discovery, SAR, modeling, and mutagenesis, J. Med. Chem. 49 (5) (2006) 1693–1705, https://doi.org/10.1021/jm051064t.
[21] E.L. Chang, C. Simmers, D.A. Knight, Cobalt complexes as antiviral and antibacterial agents, Pharmaceuticals 3 (6) (2010) 1711–1728.
[22] R. Sonq, M. Witvrouw, D. Schols, A. Robert, J. Bolzorini, E. De Clercq, J. Bernodou, B. Meunierl, Anti-HIV activities of anionic metalloporphyrins and related compounds, Antiviral Chem. Chemother. 8 (2) (1997) 85–97, https://doi.org/10.1177/095632029700800202.
[23] N. Margiotta, A. Bergamo, G. Sava, G. Padovano, E. Clercq, G. Natile, Antiviral properties and cytotoxic activity of platinum(II) complexes with 1, 10-phenanthrolines and acyclovir or penciclovir, J. Inorg. Biochem. 98 (8) (2004) 1385–1390, https://doi.org/10.1016/j.jinorgbio.2004.04.018.
[24] G. Pelosi, F. Bisceglie, F. Bignami, P. Ronzi, P. Schiavone, M.C. Re, C. Casoli, E. Pilotti, Antiretroviral activity of thiosemicarbazone metal complexes, J. Med. Chem. 53 (24) (2010) 8765–8769.
[25] V. Lorenz, P. Liebing, F. Engelhardt, F. Stein, M. Kühling, L. Schröder, F.T. Edelmann, the multicolored coordination chemistry of violurate anions, J. Coord. Chem. 72 (1) (2019) 1–34, https://doi.org/10.1080/00958972.2018.1560431.
[26] L. De Oliveira, P. Santos, J. Rubim, Raman and surface-enhanced Raman scattering of violuric acid and violurate ion adsorbed on a silver electrode, J. Raman Spectrosc. 22 (4) (1991) 197–203, https://doi.org/10.1002/jrs.1250220402.
[27] J.A. Bonacin, A.L.B. Formiga, V.H.S. de Melo, H.E. Toma, Vibrational spectra and theoretical studies of tautomerism and hydrogen bonding in the violuric acid and 6-amino-5-nitrosouracil system, Vib. Spectrosc. 44 (1) (2007) 133–141, https://doi.org/10.1016/j.vibspec.2006.10.007.
[28] W.J. Geary, The use of conductivity measurements in organic solvents for the characterization of coordination compounds, Coord. Chem. Rev. 7 (1) (1971) 81–122, https://doi.org/10.1016/S0010-8545(00)80009-0.
[29] A.W. Coats, J.P. Redfern, Kinetic parameters from thermogravimetric data, Nature 201 (4914) (1964) 68–69, https://doi.org/10.1038/201068a0.
[30] H.H. Horowitz, G. Metzger, A new analysis of thermogravimetric traces, Anal. Chem. 35 (10) (1963) 1464–1468, https://doi.org/10.1021/ac60203a013.
[31] E. KarapJnar, I.H. Gubbuk, B. Taner, P. Deveci, E. Ozcan, Thermal Degradation Behaviour of Ni(II) Complex of 3,4-Methylenedioxaphenylaminoglyoxime, J. Chem. 2013 (2013) 548067. https://doi.org/10.1155/2013/548067.
[32] D. Borah, M.K. Baruah, Kinetic and thermodynamic studies on oxidative desulphurisation of organic sulphur from Indian coal at 50–150 °C, Fuel Process. Technol. 72 (2) (2001) 83–101, https://doi.org/10.1016/S0378-3820(00)00132-6.
[33] I.T. Ahmed, Thermal decomposition study on mixed ligand thymine complexes of divalent nickel(II) with dianions of some dicarboxylic acids, J. Anal. Appl. Pyrol. 80 (2) (2007) 383–388, https://doi.org/10.1016/j.jaap.2007.04.006.
[34] K. Nakamoto, Infrared and Raman spectra of inorganic and coordination compounds, part B: applications in coordination, organometallic, and bioinorganic chemistry, John Wiley & Sons, London, 2009.

[35] R. Blinc, D. Hadži, J. Chem. Soc. (1958) 4536–4539, https://doi.org/10.1039/JR9580004536.
[36] M.J. Lacey, C. Macdonald, J. Shannon, Chelate linkage isomers of (3-Hydroxyimino-4,9-dimethyl-5, 8-diazadodeca-4,9-diene-2,11-dionato) nickel(II), Aust. J. Chem. 26 (2) (1973) 263–268, https://doi.org/10.1071/CH9730263.
[37] M.B. Cingi, A.C. Villa, A.G. Manfredotti, C. Guastini, M. Nardelli, The crystal and molecular structure of N -(1-methyl-3-oxobutylidene)- N '-(1-methyl-2-isonitroso-3-oxobutylidene) ethylenediaminecopper(II), Cu II (C12H17N3O3), Acta Crystallogr. B Struct. Sci. 28 (4) (1972) 1075–1079.
[38] K.S. Bose, C.C. Patel, Nitrosation of N, N′-ethylene bis-(acetylacetoneimine) complexes of copper(II) and nickel(II) and characterization of the products, J. Inorg. Nucl. Chem. 33 (9) (1971) 2947–2952, https://doi.org/10.1016/0022-1902(71)80057-X.
[39] M. Hamelin, Structure cristalline du violurate de strontium tetrahydrate ($C_4O_4N_3H_2$)2Sr.4H_2O, Acta Cryst. Sect. B 32(2) (1976) 364-370. https://doi.org/doi:10.1107/S0567740876012387.
[40] M.M. Aly, A.O. Baghlaf, N.S. Ganji, Linkage isomerism of the oximato group: The characterization of some mono- and binuclear square planar nickel(II) complexes of vicinal oxime-imine ligands, Polyhedron 4(7) (1985) 1301–1309. .
[41] K. Dey, K. Mandal, D. Bandyopadhyay, Hydrazones derived by the condensation of 4-methoxybenzoyl hydrazide with salicylaldehyde, ortho-hydroxyacetophenone and diacetylmonoxime, As Ligands for Cobalt (II & III), 1992.
[42] G.N. Schrauzer, R.J. Windgassen, Alkylcobaloximes and their relation to alkylcobalamins, J. Am. Chem. Soc 88 (16) (1966) 3738–3743, https://doi.org/10.1021/ja00968a012.
[43] G.N. Schrauzer, Chemie der Metall-Koordinationsverbindungen, I. Reaktion von Bis-dimethylglyoxim-nickel mit Borverbindungen, Chem. Berichte 95 (6) (1962) 1438–1445, https://doi.org/10.1002/cber.19620950620.
[44] R.M. Awadallah, A.A.M. Belal, R.M. Issa, R.D. Peacock, The colours of simple salts of the violurate anion, Spectrochim. Acta - A: Mol. Biomol. Spectrosc 47 (11) (1991) 1541–1546, https://doi.org/10.1016/0584-8539(91)80248-H.
[45] A.A. Osowole, T.I. Oni, Synthesis, characterization and antibacterial activities of some metal(II) complexes of 4-amino-2, 6-dichloropyrimidine, J. Biol. Sci. 1 (1) (2013) 32–37.
[46] M.S. Masoud, A.A. Soayed, A.E. Ali, O.K. Sharsherh, Synthesis and characterization of new azopyrimidine complexes, J. Coord. Chem. 56(8) (2003) 725. https://doi.org/0.1080/0095897031000115920.
[47] A.-E.-N.-M. Salem, A. Shawky, I.H. Badr, M.M. Khalil, Synthesis and characterization of Mn(II), Cu(II) and Cd(II) complexes of bis-Schiff bases derived from diaminonaphthalene and salicylaldehyde derivatives, Egy.J. Pure Appl. Sci. (2012) 63–70, https://doi.org/10.21608/EJAPS.2013.186243.
[48] D. Mohanabal, S. Arulantony, Synthesis, spectral characterization of schiff base complexes based on pyrimidine moiety with molecular docking with biomolecules, Asian J. Pharm. Clin. Res. 11 (10) (2018) 93–98, https://doi.org/10.22159/ajpcr.2018.v11i10.26823.
[49] A.A. Osowole, T.I. Oni, Synthesis, characterization and antibacterial activities of some metal(II) complexes of 4-amino-2, 6-dichloropyrimidine, Sci. Res. Rep. 1 (1) (2015) 32–37.
[50] A.B.P. Lever, Inorganic Electronic Spectroscopy, Elsevier, Amsterdam, 1984.
[51] K. Singh, M.S. Barwa, P. Tyagi, Synthesis and characterization of cobalt(II), nickel(II), copper(II) and zinc(II) complexes with Schiff base derived from 4-amino-3-mercapto-6-methyl-5-oxo-1,2,4-triazine, Eur. J. Med. Chem. 42 (3) (2007) 394–402, https://doi.org/10.1016/j.ejmech.2006.10.016.
[52] Y.-T. Li, C.-W. Yan, Z.-Y. Wu, C.-Y. Zhu, Synthesis and ferromagnetically coupled heterodinuclear oxamido-bridged copper(II)–oxovanadium(IV) complexes, J. Magn. Magn. Mater. 292 (2005) 418–425, https://doi.org/10.1016/j.jmmm.2004.10.119.
[53] T.A. Khan, S. Naseem, S.N. Khan, M. Shakir, Synthesis and Spectral Characterization of 14- and 16-membered tetraazamacrocyclic Schiff base ligands and their transition metal complexes and a comparative study of interaction of calf thymus DNA with copper(II) complexes, Spectrochim. Acta - A: Mol. Biomol. Spectrosc. 73 (4) (2009) 622–629, https://doi.org/10.1016/j.saa.2009.03.022.
[54] N. Raman, C. Thangaraja, S. Johnsonraja, Synthesis, spectral characterization, redox and antimicrobial activity of Schiff base transition metal(II) complexes derived from 4-aminoantipyrine and 3-salicylideneacetylacetone, Cent. Eur. J. Chem. 3 (3) (2005) 537–555, https://doi.org/10.2478/BF02479281.
[55] R.M. Kadam, M.D. Sastry, M.K. Bhide, S.A. Chavan, J.V. Yakhmi, O. Kahn, An EPR study of spin correlations and existence of ordered and disordered phases in $(NBu_4)_2Mn_2$[Cu(opba)]$_3$·6DMSO·1H_2O, Chem. Phys. Lett. 281 (4) (1997) 292–296, https://doi.org/10.1016/S0009-2614(97)01102-0.
[56] K. Jeyasubramanian, S.A. Samath, S. Thambidurai, R. Murugesan, SuthamalliK. Ramalingam, Cyclic voltammetric and e.s.r. studies of a tetraaza 14-membered macrocyclic copper (II) complex derived from 3-salicylideneacetylacetone ando-phenylenediamine: stabilization and activation of unusual oxidation states, Trans. Met. Chem. 20 (1) (1995).
[57] I. Fidone, K.W.H. Stevens, The g-value of S-state ions, Proc. Phys. Soc. 73 (1) (1959) 116–117.
[58] M.M. Ibrahim, M.A. El-Kemary, S.A. Al-Harbi, H.M. Al-Saidi, S.A. Sallam, A.-E.-M.-M. Ramadan, Synthesis and structural characterization of pyridine-based Mn(III), Fe(III), and Co(III) complexes as SOD mimics and BSA binding studies, J. Mol. Struct. 1228 (2021), https://doi.org/10.1016/j.molstruc.2020.129706 129706.
[59] A.M. Fathy, M.M. Hessien, M.M. Ibrahim, A.-E.-M.-M. Ramadan, Anionic ligands tune the structural and catalytic properties of quinoxaline-based copper(II) complexes as mimetics of copper-containing oxidase protein, J. Mol. Struct. 1250 (2022), https://doi.org/10.1016/j.molstruc.2021.131809 131809.
[60] A.E.-M.M. Ramadan, S.Y. Shaban, M.M. Ibrahim, A.-H. Adel, S.A. Sallam, S.A. Al-Harbi, W. Omar, Synthesis and spectroscopic characterization of ternary copper(II) complexes containing nitrogen and oxygen donors as functional mimics of catechol oxidase and phenoxazinone synthase, N.J.C. 44(16) (2020) 6331-6345. https://doi.org/10.1039/C9NJ06131B.
[61] H.A. Sahyon, F. Althobaiti, A.E.-M.M. Ramadan, A.M. Fathy, Quercetin - based rhodium(III) complex: Synthesis, characterization and diverse biological potentials, J. Mol. Struct. 1257 (2022), https://doi.org/10.1016/j.molstruc.2022.132584 132584.
[62] L. Yang, D.R. Powell, R.P. Houser, Structural variation in copper (I) complexes with pyridylmethylamide ligands: structural analysis with a new four-coordinate geometry index, τ_4, Dalton Trans. 9 (2007) 955–964, https://doi.org/10.1039/B617136B.
[63] M.M. Milutinović, A. Rilak, I. Bratsos, O. Klisurić, M. Vraneš, N. Gligorijević, S. Radulović, Ž.D. Bugarčić, New 4′-(4-chlorophenyl)-2,2′:6′,2″-terpyridine ruthenium(II) complexes: Synthesis, characterization, interaction with DNA/BSA and cytotoxicity studies, J. Inorg Biochem 169 (2017) 1–12, https://doi.org/10.1016/j.jinorgbio.2016.10.001.
[64] R.F. Pasternack, E.J. Gibbs, J.J. Villafranca, Interactions of porphyrins with nucleic acids, Biochemistry 22 (23) (1983) 5409–5417, https://doi.org/10.1021/bi00292a024.

[65] G. Felsenfeld, S.Z. Hirschman, A neighbor-interaction analysis of the hypochromism and spectra of DNA, J. Mol. Biol. 13 (1965) 407–427, https://doi.org/10.1016/S0022-2836(65)80106-1.
[66] J. Marmur, A procedure for the isolation of deoxyribonucleic acid from micro-organisms, J. Mol. Biol. 3 (2) (1961) 208–218, https://doi.org/10.1016/S0022-2836(61)80047-8.
[67] W.J. Mei, J. Liu, K.C. Zheng, L.J. Lin, H. Chao, A.X. Li, F.C. Yun, L.N. Ji, Experimental and theoretical study on DNA-binding and photocleavage properties of chiral complexes Δ-and Λ-[Ru (bpy) 2 L](L = o-hpip, m-hpip and p-hpip), Dalton Trans. 7 (2003) 1352–1359, https://doi.org/10.1039/B212443B.
[68] P. Krishnamoorthy, P. Sathyadevi, A.H. Cowley, R.R. Butorac, N. Dharmaraj, Evaluation of DNA binding, DNA cleavage, protein binding and in vitro cytotoxic activities of bivalent transition metal hydrazone complexes, Eur. J. Med. Chem. 46 (8) (2011) 3376–3387, https://doi.org/10.1016/j.ejmech.2011.05.001.
[69] T. Göktürk, C. Topkaya, E. Sakallı Çetin, R. Güp, New trinuclear nickel(II) complexes as potential topoisomerase I/IIα inhibitors: in vitro DNA binding, cleavage and cytotoxicity against human cancer cell lines, Chem. Pap. 76 (4) (2022) 2093–2109.
[70] A. Wolfe, G.H. Shimer, T. Meehan, Polycyclic aromatic hydrocarbons physically intercalate into duplex regions of denatured DNA, Biochem. 26 (20) (1987) 6392–6396, https://doi.org/10.1021/bi00394a013.
[71] J. Liu, H. Zhang, C. Chen, H. Deng, T. Lu, L. Ji, Interaction of macrocyclic copper(II) complexes with calf thymus DNA: effects of the side chains of the ligands on the DNA-binding behaviors, Dalton Trans. 1 (2003) 114–119, https://doi.org/10.1039/B206079P.
[72] S. Mahadevan, M. Palaniandavar, Spectroscopic and Voltammetric Studies on Copper Complexes of 2,9-Dimethyl-1,10-phenanthrolines Bound to Calf Thymus DNA, Inorg. Chem. 37 (4) (1998) 693–700, https://doi.org/10.1021/ic961066r.
[73] A.B. Tossi, J.M. Kelly, A study of some polypyridylruthenium (II) complexes as DNA binders and photocleavage reagents, Photochem. Photobiol. 49 (5) (1989) 545–556, https://doi.org/10.1111/j.1751-1097.1989.tb08423.x.
[74] J.-G. Liu, Q.-L. Zhang, X.-F. Shi, L.-N. Ji, Interaction of $[Ru(dmp)_2(dppz)]^{2+}$ and $[Ru(dmb)_2(dppz)]^{2+}$ with DNA: effects of the ancillary ligands on the DNA-binding behaviors, Inorg. Chem. 40 (19) (2001) 5045–5050, https://doi.org/10.1021/ic001124f.
[75] S. Satyanarayana, J.C. Dabrowiak, J.B. Chaires, Tris (phenanthroline)ruthenium(II) enantiomer interactions with DNA: Mode and specificity of binding, Biochemistry 32 (10) (1993) 2573–2584, https://doi.org/10.1021/bi00061a015.
[76] G. Li, E. De Clercq, Therapeutic options for the 2019 novel coronavirus (2019-nCoV), Nat. Rev. Drug Discovery 19 (3) (2020) 149–150, https://doi.org/10.1038/d41573-020-00016-0.
[77] J.C. Crosby, M.A. Heimann, S.L. Burleson, B.C. Anzalone, J.F. Swanson, D.W. Wallace, C.J. Greene, COVID-19: a review of therapeutics under investigation, J. Am. Coll. Emerg. Phys. Open 1 (3) (2020) 231–237, https://doi.org/10.1002/emp2.12081.
[78] J.S. Morse, T. Lalonde, S. Xu, W.R. Liu, Learning from the past: possible urgent prevention and treatment options for severe acute respiratory infections caused by 2019-nCoV, ChemBioChem 21 (5) (2020) 730–738, https://doi.org/10.1002/cbic.202000047.
[79] M. Jawaid Akhtar, COVID19 inhibitors: A prospective therapeutics, Bioorg. Chem. 101 (2020), https://doi.org/10.1016/j.bioorg.2020.104027 104027.
[80] R.E. de Paiva, A.M. Neto, I.A. Santos, A.C. Jardim, P.P. Corbi, F.R. Bergamini, What is holding back the development of antiviral metallodrugs? A literature overview and implications for SARS-CoV-2 therapeutics and future viral outbreaks, Dalton Trans. 49 (45) (2020) 16004–16033, https://doi.org/10.1039/D0DT02478C.
[81] E.J. Anthony, E.M. Bolitho, H.E. Bridgewater, O.W.L. Carter, J.M. Donnelly, C. Imberti, E.C. Lant, F. Lermyte, R.J. Needham, M. Palau, P.J. Sadler, H. Shi, F.-X. Wang, W.-Y. Zhang, Z. Zhang, Metallodrugs are unique: opportunities and challenges of discovery and development, Chem. Sci. 11 (48) (2020) 12888–12917, https://doi.org/10.1039/D0SC04082G.
[82] E. Boros, P.J. Dyson, G. Gasser, Classification of metal-based drugs according to their mechanisms of action, Chem 6 (1) (2020) 41–60, https://doi.org/10.1016/j.chempr.2019.10.013.
[83] K.D. Mjos, C. Orvig, Metallodrugs in medicinal inorganic chemistry, Chem. Rev. 114 (8) (2014) 4540–4563, https://doi.org/10.1021/cr400460s.
[84] J. Karges, Combining inorganic chemistry and biology: The underestimated potential of metal complexes in medicine, ChemBioChem 21 (21) (2020) 3044–3046, https://doi.org/10.1002/cbic.202000397.
[85] S.M. Meier-Menches, C. Gerner, W. Berger, C.G. Hartinger, B. K. Keppler, Structure–activity relationships for ruthenium and osmium anticancer agents–towards clinical development, Chem. Soc. Rev. 47 (3) (2018) 909–928, https://doi.org/10.1039/C7CS00332C.
[86] J. Karges, R.W. Stokes, S.M. Cohen, Metal complexes for therapeutic applications, Trends Chem. 3 (7) (2021) 523–534, https://doi.org/10.1016/j.trechm.2021.03.006.
[87] Y.C. Ong, S. Roy, P.C. Andrews, G. Gasser, Metal compounds against neglected tropical diseases, Chem. Rev. 119 (2) (2019) 730–796, https://doi.org/10.1021/acs.chemrev.8b00338.
[88] M.N.A. Bitu, M.S. Hossain, A. Zahid, C. Zakaria, M. Kudrat-E-Zahan, Anti-pathogenic activity of cu (II) complexes incorporating Schiff bases: a short review, Am. J. Heterocycl. Chem. 5 (1) (2019) 11–23, https://doi.org/10.11648/j.ajhc.20190501.14.
[89] A.M. Ramadan, Structural and biological aspects of copper (II) complexes with 2-methyl-3-amino-(3H)-quinazolin-4-one, J. Inorg. Biochem. 65 (3) (1997) 183–189, https://doi.org/10.1016/S0162-0134(96)00122-5.
[90] B. Tweedy, Plant extracts with metal ions as potential antimicrobial agents, Phytopathology 55 (1964) 910–914.